Keratin 1 maintains skin integrity and participates in an inflammatory network in skin through interleukin-18

Wera Roth[1], Vinod Kumar[1], Hans-Dietmar Beer[2], Miriam Richter[1], Claudia Wohlenberg[3], Ursula Reuter[3], Sören Thiering[1], Andrea Staratschek-Jox[4], Andrea Hofmann[4], Fatima Kreusch[4], Joachim L. Schultze[4], Thomas Vogl[5], Johannes Roth[5], Julia Reichelt[6], Ingrid Hausser[7] and Thomas M. Magin[1,*]

[1]Translational Centre for Regenerative Medicine (TRM) and Institute of Biology, University of Leipzig, 04103 Leipzig, Germany
[2]University Hospital, Department of Dermatology, University of Zurich, 8006 Zurich, Switzerland
[3]Institute of Biochemistry and Molecular Biology, Division of Cell Biochemistry, University of Bonn, 53115 Bonn, Germany
[4]Department of Genomics and Immunoregulation, LIMES Institute, University of Bonn, 53115 Bonn, Germany
[5]Institute of Immunology, University of Münster, 48149 Münster, Germany
[6]Institute of Cellular Medicine and North East England Stem Cell Institute, Newcastle University, Newcastle upon Tyne NE2 4HH, UK
[7]Universitäts-Hautklinik, Ruprecht-Karls-Universität Heidelberg, 69120 Heidelberg, Germany
*Author for correspondence (thomas.magin@trm.uni-leipzig.de)

Accepted 8 October 2012
Journal of Cell Science 125, 5269–5279

doi: 10.1242/jcs.116574

Summary

Keratin 1 (KRT1) and its heterodimer partner keratin 10 (KRT10) are major constituents of the intermediate filament cytoskeleton in suprabasal epidermis. KRT1 mutations cause epidermolytic ichthyosis in humans, characterized by loss of barrier integrity and recurrent erythema. In search of the largely unknown pathomechanisms and the role of keratins in barrier formation and inflammation control, we show here that Krt1 is crucial for maintenance of skin integrity and participates in an inflammatory network in murine keratinocytes. Absence of Krt1 caused a prenatal increase in interleukin-18 (IL-18) and the S100A8 and S100A9 proteins, accompanied by a barrier defect and perinatal lethality. Depletion of IL-18 partially rescued *Krt1*$^{-/-}$ mice. IL-18 release was keratinocyte-autonomous, KRT1 and caspase-1 dependent, supporting an upstream role of KRT1 in the pathology. Finally, transcriptome profiling revealed a Krt1-mediated gene expression signature similar to atopic eczema and psoriasis, but different from Krt5 deficiency and epidermolysis bullosa simplex. Our data suggest a functional link between KRT1 and human inflammatory skin diseases.

Key words: Keratin cytoskeleton, Epidermal barrier, Innate immunity, Interleukin-18, Atopic eczema

Introduction

The epidermis protects an organism against mechanical injury and dehydration, and regulates immune homeostasis by virtue of epidermal keratinocytes (Simpson et al., 2011). Many of its functions depend on structural proteins including keratins (Kim and Coulombe, 2007; Magin et al., 2007). Keratins constitute the intermediate filament cytoskeleton in all epithelia (Schweizer et al., 2006). The type II keratin KRT1 and its heterodimer type I partner KRT10 form the major cytoskeleton in suprabasal keratinocytes. Their upregulation precedes expression of filaggrin and cornified envelope proteins. Covalent crosslinking of Krt1 but not Krt10 to these proteins, in addition to a complex series of lipids, ultimately forms the cornified/lipid envelope, which, together with Langerhans cells, constitutes the epidermal barrier (Candi et al., 2005; Simpson et al., 2011). This led to the hypothesis that a subset of keratins and the associated protein filaggrin are crucial for barrier function. In fact, KRT1 and KRT10 mutations lead to congenital epidermolytic ichthyosis (EI, MIM 113800) characterized by skin erosions, hyperkeratosis and barrier defects (Arin et al., 2011; Lane and McLean, 2004; Schmuth et al., 2001; Segre, 2006), whereas mutations in filaggrin can cause the inflammatory disorder atopic eczema (AE) (Brown and McLean, 2012; Oji et al., 2010). EI is characterized by skin erosions, hyperkeratosis and barrier defects (Lane and McLean, 2004; Schmuth et al., 2001; Segre, 2006). Although these disorders have established a primary role of keratinocyte-resident proteins in acute and chronic skin diseases (Brown and McLean, 2012; Nestle et al., 2009; Quigley et al., 2009), the underlying pathomechanisms remain poorly understood.

Besides immune cells, keratinocytes regulate skin inflammatory and immune responses by secretion of cytokines, antimicrobial peptides and by expression of MHCII proteins (Nestle et al., 2009). S100A8 and A9 proteins belong to the S100 family of calcium-binding proteins that can act as antimicrobial peptides and are released as heterodimers upon barrier defects by unconventional secretion. Once released, they act as autocrine activators of Toll-like receptor (TLR) 4 on keratinocytes (Eckert et al., 2004; Ehrchen et al., 2009; Nestle et al., 2009; Vogl et al., 2007). They are elevated in psoriatic skin and therefore are linked to inflammatory skin diseases (Nestle et al., 2009). Interleukins (IL) IL-18 and IL-33 are pro-inflammatory cytokines of the IL-1 family produced by suprabasal keratinocytes (Dinarello, 2009). Skin-specific overexpression of IL-18 in mice results in AE-like inflammatory lesions (Konishi et al., 2002), and IL-18 levels are elevated in humans suffering from AE (Kou et al., 2012). IL-18 is synthesized with an N-terminal propeptide requiring cleavage by caspase-1 or other proteases before unconventional secretion from a variety of cells, including keratinocytes (Dinarello, 2009). Activation of caspase-1 is tightly regulated by the inflammasome,

Journal of Cell Science

a large cytoplasmic multiprotein complex consisting of scaffold proteins such as NLRP3 in keratinocytes, the adaptor protein ASC (apoptosis-associated speck-like protein containing a caspase recruitment domain) and procaspase-1/-5 (Davis et al., 2011). The mechanisms controlling inflammasome activation are partially understood and include TLRs, sensing either pathogen-associated molecular patterns (PAMPs) or NOD and RIG receptors, recognizing self-derived danger signals, including nucleic acids, ATP, cholesterol crystals and amyloid beta (Davis et al., 2011). An intriguing question is whether the keratinocyte cytoskeleton is involved in intracellular damage control.

To test this hypothesis, we have generated *Krt1*$^{-/-}$ mice. In contrast to Krt10 deficiency, which led to viable mice with a mild phenotype (Reichelt et al., 2001), loss of Krt1 caused perinatal lethality and a barrier defect. Transcriptional profiling revealed a gene expression signature in *Krt1*$^{-/-}$ skin similar to the human inflammatory skin diseases AE and psoriasis. Depletion of IL-18 partially rescued *Krt1*$^{-/-}$ mice. Our data identify keratin proteins as gatekeepers of immune responses in skin and link cytokine release to the loss of KRT1.

Results

Krt1 controls the skin barrier

To address isotype-specific keratin functions during epidermal differentiation and barrier formation (Kim and Coulombe, 2007; Magin et al., 2007) we generated Krt1-deficient mice (Fig. 1B,D; supplementary material Fig. S1B). Surprisingly, the absence of Krt1 caused neonatal lethality in a mixed 129/Ola×C57BL/6 genetic background, unlike Krt10 depletion (Reichelt et al., 2001). Histology of neonatal *Krt1*$^{-/-}$ skin revealed a largely intact stratified epidermis, without local inflammation and localized keratinocyte lesions, possibly from handling-induced trauma. Further, the granular layer was reduced (Fig. 1A). Expression of Krt10, the obligate heterodimer protein partner of Krt1, was significantly reduced in *Krt1*$^{-/-}$ skin extracts, but its intracellular distribution remained unaltered (Fig. 1C,D). Electron microscopy revealed sparse keratin aggregates in *Krt1*$^{-/-}$ skin due to loss of Krt1, indicating lack of compensatory keratins, and normal filaments in wild-type epidermis (supplementary material Fig. S1A). Krt5 and Krt14, typically restricted to basal keratinocytes, were present in suprabasal *Krt1*$^{-/-}$ skin, and their protein level was slightly elevated, similar to other epidermis-specific knockouts (supplementary material Fig. S1C–E). In *Krt10*$^{-/-}$ mice, no Krt1 aggregates were detectable, but atypical intermediate filament between Krt1 and Krt14 were present and contributed to skin integrity (Reichelt et al., 2001). To address whether Krt10 assembled with type II keratins Krt5 or Krt6 in *Krt1*$^{-/-}$ epidermis, high resolution confocal imaging was performed. This revealed the presence of numerous Krt10 aggregates without Krt5 or Krt6 in spinous layer keratinocytes, indicating that upon expression of Krt10, no type II partner is available to form intermediate filaments (Fig. 2A,B). In the absence of Krt1, the distribution and staining intensity of major desmosomal proteins desmoplakin, desmoglein1 and 2 and plakoglobin were unaffected (Fig. 2C–E). This suggested that both presence and intracellular organization of Krt5/14 filaments in suprabasal epidermis maintained desmosome functionality. Distribution and expression levels of cornified envelope (CE) proteins loricrin, involucrin and filaggrin (supplementary material Fig. S1F; Fig. S2B, and data not shown) appeared unaltered, supporting occurrence of terminal differentiation. A strong hint on disturbed skin homeostasis came from the appearance of stress-associated Krt6 and Krt16, induced upon hyperproliferation,

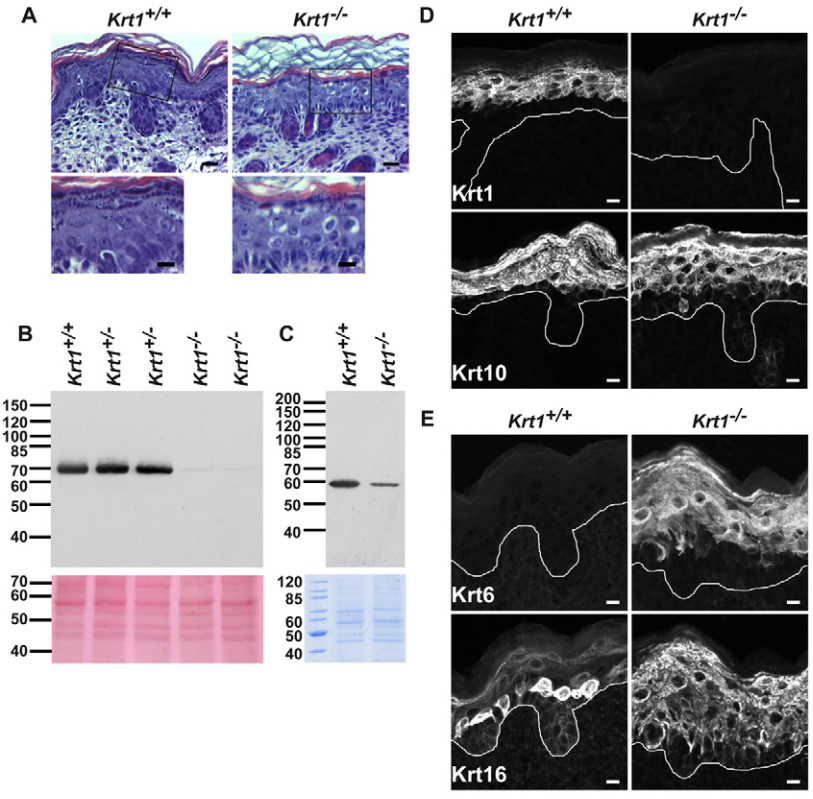

Fig. 1. *Krt1*$^{-/-}$ mice show an overall intact epidermis and a normal morphology. (**A**) Hematoxylin/Eosin-stained full-thickness back skin sections from *Krt1*$^{+/+}$ and *Krt1*$^{-/-}$ pups at P0. Scale bars: top, 20 μm; bottom, 10 μm. (**B**,**C**) Immunoblot analysis of Krt1 (B) and Krt10 (C) expression in total skin extracts from *Krt1*$^{+/+}$ and *Krt1*$^{-/-}$ pups at P0. Equal loading was assessed by Ponceau S staining of the blotted protein on nitrocellulose membranes (B) or Coomassie staining of SDS-polyacrylamide gels run in parallel (C). Molecular mass standards are indicated in kDa. (**D**) Immunofluorescence staining of full-thickness back skin sections from *Krt1*$^{+/+}$ and *Krt1*$^{-/-}$ pups at P0 with antibodies against Krt1 and Krt10. The solid line indicates the basement membrane. Scale bars: 10 μm. (**E**) Immunofluorescence staining of full-thickness back skin sections from *Krt1*$^{+/+}$ and *Krt1*$^{-/-}$ pups at P0 with antibodies against Krt6 and Krt16. Solid line indicates basement membrane. Scale bars: 10 μm.

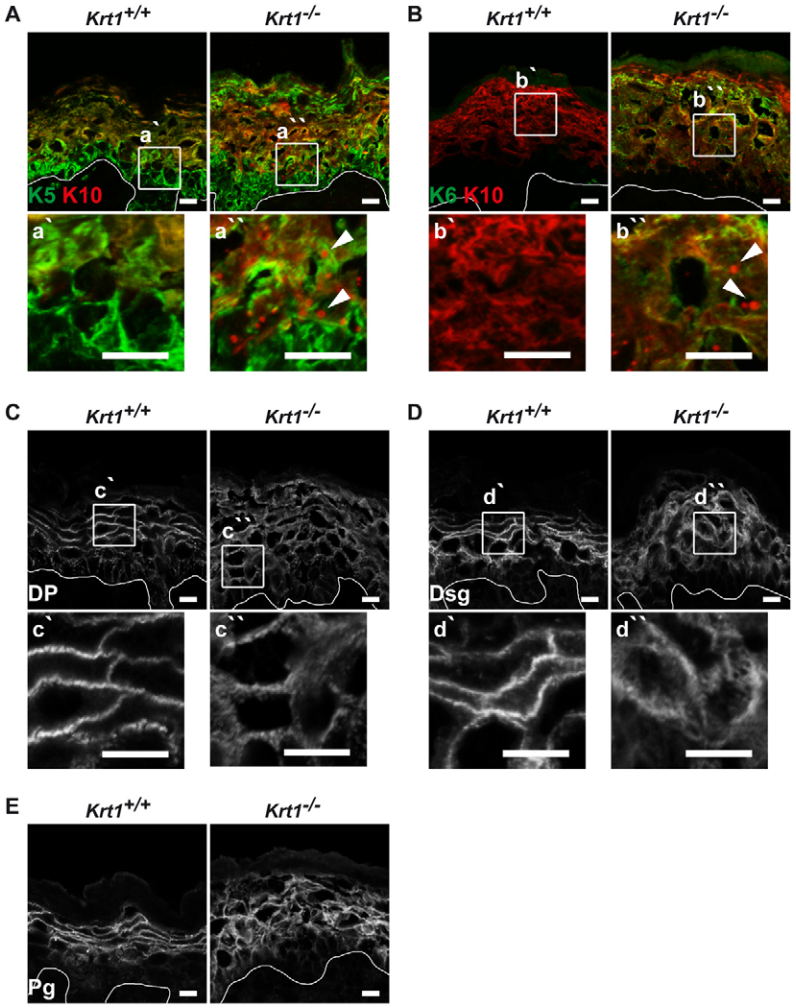

Fig. 2. Exclusion of Krt5 and Krt6 from K10 aggregates and unaltered desmosome distribution in *Krt1*$^{-/-}$ mice. (**A**,**B**) Double immunofluorescence staining of full-thickness back skin sections from *Krt1*$^{+/+}$ and *Krt1*$^{-/-}$ pups at P0 with antibodies against Krt5 and Krt10 (A) or against Krt6 and Krt10 (B). The solid line indicates the basement membrane. Lower panels a′, a″, b′, b″ are magnified images of the boxed regions in the upper panels. Note the absence of Krt5 or Krt6 in Krt10 aggregates. Scale bars: 10 μm. (**C**–**E**) Immunofluorescence staining of full-thickness back skin sections from *Krt1*$^{+/+}$ and *Krt1*$^{-/-}$ pups at P0 showing the distribution of desmoplakin (C; DP), desmoglein (D; Dsg) and plakoglobin (E; Pg). The solid line indicates the basement membrane. Lower panels c′, c″, d′, d″ are magnified images of the boxed regions in the upper panels. Note unaltered colocalization and distribution of major desmosomal proteins in the absence of Krt1. Scale bars: 10 μm.

barrier defects and wound healing (Kim and Coulombe, 2007) (Fig. 1E; supplementary material Fig. S1C). The mild skin defects of *Krt1*$^{-/-}$ mice and the notion that *Krt1*$^{-/-}$, in contrast to *Krt10*$^{-/-}$ mice, are not viable (Reichelt et al., 2001; Reichelt and Magin, 2002), point to a novel and unique function of Krt1 *in vivo*. This is also in agreement with the recently described phenotype of Krt1/10 doubly deficient mice (Wallace et al., 2012).

The known participation of KRT1, but not KRT10 to cornified envelope formation (Candi et al., 2005; Candi et al., 1998) and a mild weight loss of *Krt1*$^{-/-}$ mice that manifested postnatally (supplementary material Fig. S2A) prompted us to examine epidermal barrier integrity employing an established dye-penetration assay (Segre et al., 1999). This established an intact outside-in epidermal barrier in *Krt1*$^{-/-}$ newborns, as no dye penetrated the skin (Fig. 3A). In contrast, trans-epidermal water loss (TEWL) was increased twofold in neonatal *Krt1*$^{-/-}$ mice, revealing a defective inside-out barrier (Fig. 3D). Possibly, the biotin assay performed in Krt1/10-doubly-deficient mice may not fully reveal the barrier state of these mice (Wallace et al., 2012). Furthermore, the number of intact cornified envelopes was significantly reduced to ~17% in *Krt1*$^{-/-}$ compared to ~84% in *Krt1*$^{+/+}$ and ~55% in *Krt10*$^{+/+}$mouse skins (Fig. 3B,C,E; supplementary material Fig. S2C,D). Together with the notion that in Krt1/10 doubly deficient mice 60% of cornified envelopes remained intact (Wallace et al., 2012), our data substantiated a major role of the type II Krt1 in barrier integrity. To address the known role of tight junctions which contribute to barrier functionality by sealing the paracellular spaces between granular layer keratinocytes (Kubo et al., 2012), tight junction protein expression and distribution were examined. The unaltered expression of claudin-1 (Cldn), Cldn4 and Cldn5 (Fig. 3F) and of ZO-1 and occludin (data not shown) in *Krt1*$^{-/-}$ mice further supported a primary defect directly related to Krt1.

Krt1 links barrier function to inflammation and innate immunity

To unravel previously unnoted and essential functions of Krt1 at the molecular level, we performed global gene expression analysis on back skin from *Krt1*$^{-/-}$ mice and *Krt1*$^{+/+}$ littermates at the onset of Krt1 expression [embryonic day (E)15.5], at E18.5 and at postnatal (P) day 0. At E15.5, when Krt1 expression commences during mouse development, Krt1 itself was the only gene differentially expressed in the two genotypes (data not shown). At E18.5, we found 163 genes upregulated and only two genes downregulated in *Krt1*$^{-/-}$ skin. In newborn skin, 627 genes were upregulated and 284 were downregulated in *Krt1*$^{-/-}$ mice. Gene set enrichment analysis,

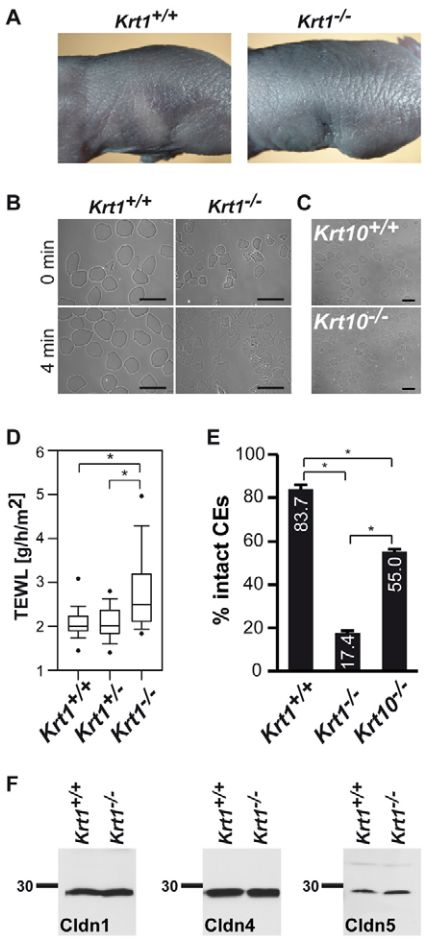

Fig. 3. *Krt1*$^{-/-}$ mice have an epidermal barrier defect. (**A**) Toluidine blue dye exclusion assay of *Krt1*$^{+/+}$ and *Krt1*$^{-/-}$ pups at P0. (**B**) Gross morphology of CEs from *Krt1*$^{+/+}$ and *Krt1*$^{-/-}$ skin at P0 after sonification for 0 or 4 min. Scale bars: 100 μm. (**C**) Gross morphology of CEs from *Krt10*$^{+/+}$ and *Krt10*$^{-/-}$ skin at P0. Scale bars: 100 μm. (**D**) Box and whisker plot of transepidermal water loss (TEWL) of *Krt1*$^{+/+}$ (n=38), *Krt1*$^{+/-}$ (n=83) and *Krt1*$^{-/-}$ (n=43) pups at P0. The median and the 5th and 95th percentile are shown. *P<0.05. (**E**) Quantitative analysis of intact versus fragile CEs at P0 from three mice per genotype. Values are means ± s.e.m. *P<0.05. (**F**) Immunoblot analysis of Cldn1, Cldn4 and Cldn5 expression in total skin extracts from *Krt1*$^{+/+}$ and *Krt1*$^{-/-}$ pups at P0. Equal loading was assessed by Ponceau S staining of the proteins blotted on nitrocellulose membranes (not shown). Molecular mass standards are indicated in kDa. Note unaltered amounts of claudins in both genotypes of mice.

followed by gene ontology classification and grouping according to function (Keller et al., 2008) of genes upregulated in *Krt1*$^{-/-}$ skin revealed a similar distribution of function categories in E18.5 and newborn samples (supplementary material Fig. S3A,B). Strikingly, cluster analysis and heat maps identified a significant over-representation of genes linked to CE formation/epidermal differentiation (Fig. 4A,C) and inflammatory/immune defense pathways (Fig. 4B,D) in E18.5 and newborn *Krt1*$^{-/-}$ skin, demonstrating that both gene sets were altered prenatally. To validate array data, selected candidate gene expression was confirmed by quantitative RT-PCR (supplementary material Fig. S3C–E). Prenatal upregulation of pro-inflammatory genes strongly supported a direct involvement of Krt1 in the regulation of the above pathways. The pattern of genes upregulated in *Krt1*$^{-/-}$ skin, e.g. Il-1β, IL-18, defensins and S100 proteins, bore resemblance to the human inflammatory skin diseases atopic eczemia (AE) and psoriasis, characterized by barrier defects, inflammation and immune dysregulation (Barnes, 2010; Gudjonsson et al., 2010; Gudjonsson et al., 2009; Sääf et al., 2008; Suárez-Fariñas et al., 2010; Suárez-Fariñas et al., 2011). We then focused on IL-18, as cytokine analysis of E18.5 serum samples confirmed its elevation (see below, Fig. 5A). To substantiate this further, global comparisons between the *Krt1* data set (our study) and genome-wide transcriptional profiling data sets derived from AE and psoriasis patients were performed (Gudjonsson et al., 2010; Sääf et al., 2008). The intersection of similarly regulated genes in *Krt1*$^{-/-}$ skin and AE or psoriatic skin was remarkably high: 55 (E18.5) and 154 (P0) genes similar to AE skin, and 86 (E18.5) and 166 genes (P0) similar to psoriatic skin (Fig. 4E; supplementary material Tables S1, S2). Genes similarly regulated in *Krt1*$^{-/-}$ and AE skin are *IL-18*, *S100A8/A9*, *Il6/Il6R*, *SOCS3*, *KLK*, *TGM* and *SPRR* (supplementary material Tables S1, S2), genes that have been described to be associated with AE (Barnes, 2010; Sääf et al., 2008; Suárez-Fariñas et al., 2011). In analogy, genes upregulated in *Krt1*$^{-/-}$ and psoriatic skin were compared. This uncovered a group of genes previously ascribed to psoriasis, including epidermal barrier-coding genes, e.g. *SPRRs*, *S100*, *KLKs*, *IL-1* family members and genes of lipid metabolism (*ELOV* and fatty acid binding protein, *FABP*) (Gudjonsson et al., 2010; Gudjonsson et al., 2009; Suárez-Fariñas et al., 2010) (supplementary material Tables S1, S2). In striking contrast, the comparison of genes upregulated in *Krt1*$^{-/-}$ versus *Krt5*$^{-/-}$ mouse skin, which serves as a model for the keratin-associated disease epidermolysis bullosa simplex (EBS) was very low, with 14 genes at E18.5 and 23 genes at P0 (Lu et al., 2007) (Fig. 4E). Furthermore, only 11 upregulated genes at E18.5 and 18 genes at P0 in *Krt1*$^{-/-}$ skin were common to human EBS patient skin (Bchetnia et al., 2012). Based on these data we conclude that the gene expression signature from *Krt1*$^{-/-}$ mice shows more similarities to human inflammatory skin diseases than to keratin-associated defects in mice and humans (supplementary material Table S3).

To further dissect the role of Krt1 in inflammation, gene set enrichment analysis (GSEA) was performed to identify commonly regulated pathways in *Krt1*$^{-/-}$ versus AE and *Krt1*$^{-/-}$ versus psoriatic skin. Remarkably, the pathway network obtained for the *Krt1*$^{-/-}$ versus AE intersection (Fig. 4F; supplementary material Tables S4, S5) showed a striking similarity to the AE pathway. Resulting data were compared with an ingenuity pathway analysis based on 81 validated AE genes (Barnes, 2010), which detects expression patterns of genes whose expression is linked to distinct signaling pathways. This highlighted the functional significance of IL-1 family members such as IL-18, TLR/MYD88 signaling, and NOD-like receptor family members (NLR) in *Krt1*$^{-/-}$ mice and in AE. In contrast, the pathway network obtained for the *Krt1*$^{-/-}$ versus psoriasis intersection was less extended and showed a limited interconnection of functional clusters (data not shown). These data suggested a link between Krt1 and IL-18.

Krt1 restrains inflammation and innate immunity in skin

To further substantiate Krt1 involvement in an inflammatory network in keratinocytes, we focused on IL-18 and related pro-inflammatory cytokines. Quantitative RT-PCR showed a significant upregulation of IL-18 in E18.5 *Krt1*$^{-/-}$ skin

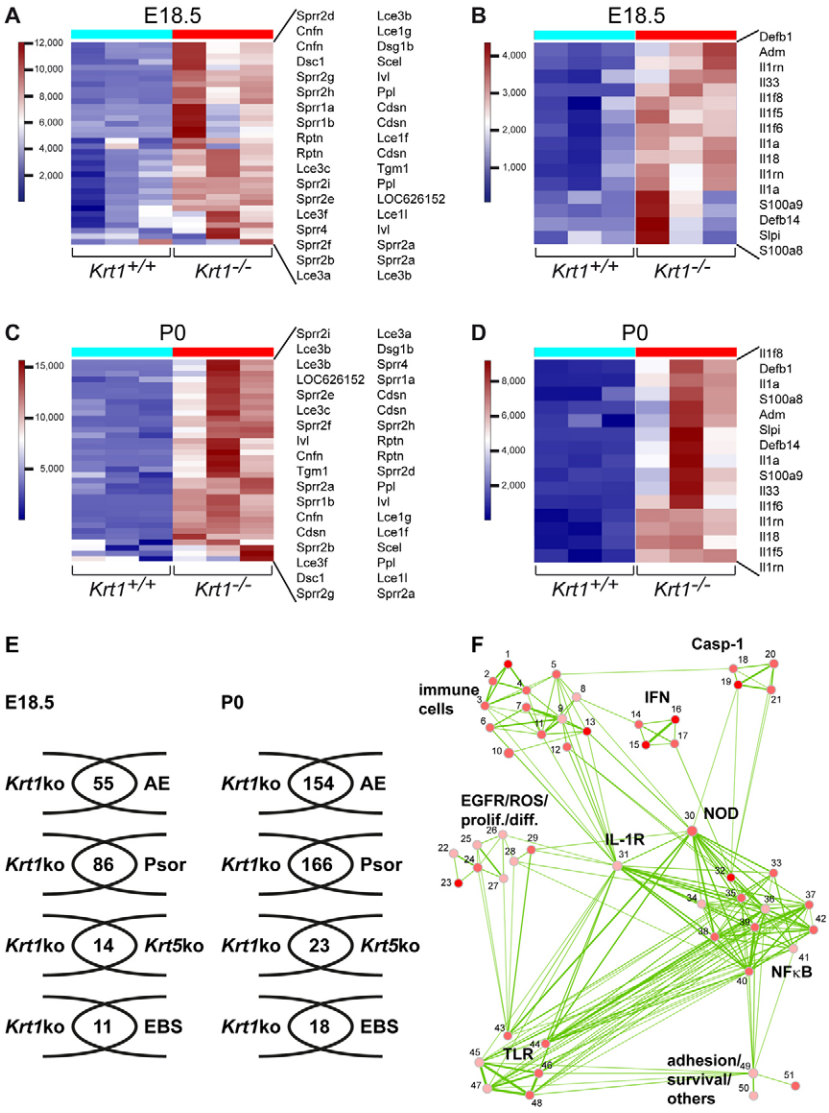

Fig. 4. Functional barrier defects coincide with activation of innate immune response genes in *Krt1*$^{-/-}$ mice which establish prenatally and overlap with differentially expressed genes linked to human inflammatory skin diseases. (**A–D**) Cluster analysis and heat maps of differentially expressed genes in *Krt1*$^{-/-}$ skin at E18.5 (A,B) and P0 (C,D) associated with CE formation (A,C) and linked to immune response pathways (B,D). Samples from three mice per genotype were analyzed. Red indicates genes upregulated in *Krt1*$^{-/-}$ compared with *Krt1*$^{+/+}$ skin. (**E**) Global comparison analyses performed between the *Krt1* data set and genome-wide transcriptional profiling data sets derived from AE, psoriasis and EBS patients and the data set from the *Krt5*-targeted EBS mouse model, respectively. Shown are the numbers of identical gene identifiers present in the intersection of respective comparison analyses. (**F**) Interconnected network of common regulated pathways present in both *Krt1*$^{-/-}$ versus AE skin, based on gene set enrichment analyses (GSEA) using the MSigDB database. The top 100 enriched pathways with a $P<0.001$ were used, and the resulting pathway network of fully connected gene sets (cliques) grouped according to functional clusters are shown. Depicted gene sets of the clusters are numbered and corresponding pathway IDs are listed in supplementary material Table S4 (see supplementary material Table S5 for details) (Merico et al., 2010).

(supplementary material Fig. S3D), consistent with its marked elevation at the protein level in suprabasal, neonatal *Krt1*$^{-/-}$ skin and in the dermis (Fig. 5A). Moreover, IL-18 levels were significantly elevated in the serum of newborn *Krt1*$^{-/-}$ mice (Fig. 5D). In line with the AE-like phenotype resulting from ectopic expression of IL-18 in mouse epidermis and the recent identification of high serum IL-18 in AE patients (Kambe et al., 2010; Konishi et al., 2002; Kou et al., 2012), our data support a role of IL-18 in the pathology of *Krt1*$^{-/-}$ mice. Furthermore, the levels of IL-33, another member of the IL-1 family, were markedly increased in epidermal extracts of *Krt1*$^{-/-}$ mice, but only mildly increased in newborn *Krt1*$^{-/-}$ serum (Fig. 5D). IL-33 is known to be expressed in the suprabasal epidermis and the lung where it mediates a pro-inflammatory response by activating mast cells and Th2 lymphocytes. Its upregulation has been associated with allergic airway diseases and asthma (Haraldsen et al., 2009). The antimicrobial peptides S100A8 and S100A9, two damage-associated molecular pattern (DAMP) molecules linked to compromised skin barrier function and inflammatory skin diseases (Ehrchen et al., 2009), were strongly induced in suprabasal *Krt1*$^{-/-}$ epidermis, where Krt1 is normally expressed, but also in the dermis, supporting an inflammatory response (Fig. 5B,D). Moreover, thymic stromal lymphopoietin (TSLP), a cytokine produced by differentiated keratinocytes (Ziegler and Artis, 2010), was increased in *Krt1*$^{-/-}$ epidermal extracts (supplementary material Fig. S4C). TSLP has been implicated in atopic dermatitis and is a master switch for allergic inflammatory airway diseases in mice (Ziegler and Artis, 2010). The elevated expression of these cytokines in *Krt1*$^{-/-}$ mice and in AE (Ehrchen et al., 2009; Suárez-Fariñas et al., 2011) lends further support to a role of Krt1 in controlling skin inflammation.

Next, we examined whether elevated cytokine levels might be connected to erythema and to additional systemic defects noted in epidermolytic ichthyosis (Arin et al., 2011). Staining for platelet endothelial cell adhesion molecule (PECAM) was increased, indicating increased vascularization at the dermal/epidermal interface (Fig. 5C; supplementary material Fig. S4A,B). In line with these findings, lungs from P0 *Krt1*$^{-/-}$ pups had higher blood cell numbers (supplementary material Fig. S4D,E) and displayed capillary leakage (supplementary material Fig. S4F).

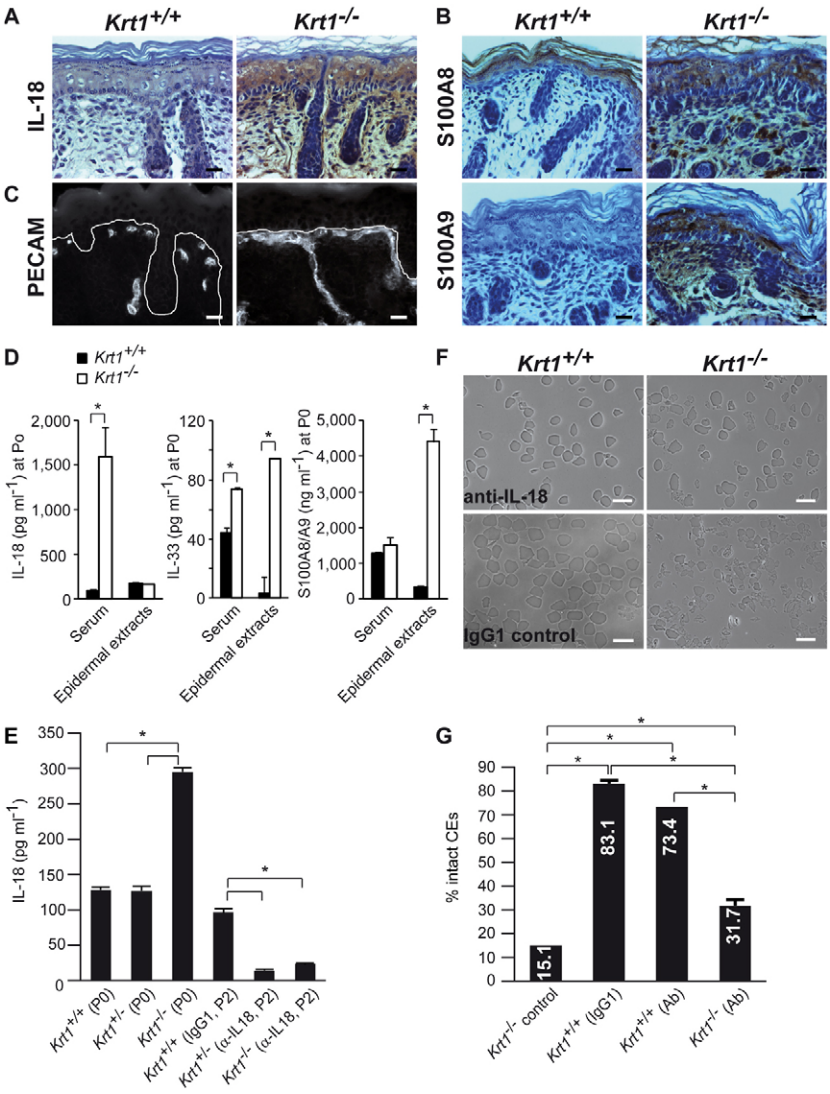

Fig. 5. Upregulation of Il-18 and S100A8/A9 in skin results in a systemic IL-18 release and the $Krt1^{-/-}$ phenotype can be partially rescued by injection of IL-18 blocking antibodies. (**A**,**B**) Immunohistochemistry for IL-18 (A) and S100A8, S100A9 (B) in full-thickness back-skin sections from $Krt1^{+/+}$ and $Krt1^{-/-}$ pups at P0. Scale bars: 20 µm. (**C**) Immunofluorescence staining of blood vessels with PECAM antibodies in back-skin sections of $Krt1^{-/-}$ and $Krt1^{+/+}$ mice at P0. The solid line indicates the basement membrane. Scale bars: 20 µm. (**D**) ELISA analysis of IL-18, IL-33 and S100A8/A9 in newborn serum (P0) and epidermal protein extracts. Values are means ± s.d. of duplicate measurements of pooled sera ($Krt1^{+/+}$, n=28; $Krt^{-/-}$, n=28) and epidermal extracts (n=6 for both genotypes). *P<0.05. (**E**) IL-18 ELISA of serum samples from $Krt1^{-/-}$ and $Krt1^{+/+}$ mice at P2 either treated with an anti-IL-18-blocking antibody or mock treated. Values are means ± s.e.m. of duplicate or triplicate measurements of pooled sera (n=3–12 mice). *P<0.05. (**F**) Gross morphology of CEs from $Krt1^{+/+}$ and $Krt1^{-/-}$ skin at P2 after anti-IL-18 blocking antibody treatment. Scale bars: 100 µm. (**G**) Quantitative analysis of intact versus fragile CEs at P2 after treatment with IL-18-blocking antibodies ($Krt1^{+/+}$ IgG1, n=3; $Krt1^{+/+}$ anti-IL-18, n=1; $Krt1^{-/-}$ anti-IL-18, n=3; $Krt1^{-/-}$ vehicle, n=1 due to early neonatal lethality of untreated $Krt1^{-/-}$ mice). Values are means ± s.e.m. *P<0.05.

Finally, the expression of the prominent pro-inflammatory cytokines IL-1α and TNFα remained unaltered in $Krt1^{-/-}$ mice (data not shown), underscoring the selectivity of Krt1 function.

Pharmacological and genetic ablation of IL-18 rescues the Krt1 phenotype

To validate our hypothesis that KRT1 restrains inflammation and an innate response in the epidermis by promoting barrier acquisition and restricting IL-18 release, we decided on a rescue of $Krt1^{-/-}$ mice following antibody-mediated depletion and loss-of-function approaches. Surprisingly, systemic administration of IL-18-blocking antibodies to pregnant females extended the lifespan of $Krt1^{-/-}$ pups for at least 2 days. The antibody-mediated IL-18 blockade (Fig. 5E–G; supplementary material Fig. S4G) increased the percentage of intact CEs (~32% versus ~15% in isotype-treated controls), indicating a crucial role of IL-18. To gather additional evidence, a genetic rescue experiment was conducted, crossing $Krt1^{-/-}$ to $Il18^{-/-}$-knockout mice (Hochholzer et al., 2000). Double heterozygous $Krt1^{+/-}Il18^{+/-}$ mice were interbred and offspring that survived until 4- to 6-weeks of age were assessed for homozygosity. Loss of IL-18 resulted in a partial rescue of $Krt1^{-/-}$ mice, since 12 $Krt1^{-/-}Il18^{-/-}$ survivors were obtained from 16 expected survivors (75%), compared with only six $Krt1^{-/-}Il18^{+/+}$ expected from 16 survivors (37.5%) in a *Il18* wild-type genetic background (Fig. 6A). In contrast, the equivalent rescue experiment using a S100A9-deficient background (Manitz et al., 2003) generated no survivors (data not shown). Rescued $Krt1^{-/-}Il18^{-/-}$ double-deficient mice exhibited an apparently normal epidermal morphology similar to $Krt1^{-/-}$ mice (Fig. 6B,C; supplementary material Fig. S5D,E). Analysis of cornified envelopes revealed a twofold increase in intact CEs in newborn $Krt1^{-/-}Il18^{-/-}$ skin compared with corresponding $Krt1^{-/-}$ skin at P0, in line with the results obtained by the antibody blocking experiment (Fig. 6D,E; supplementary material Fig. S5A–C). Thus, we conclude that Krt1 acts upstream of IL18.

IL-18 release is mediated by caspase-1 in a Krt1-dependent manner

Having established a major role of IL-18 in Krt1 pathology, we sought to identify the underlying mechanism responsible for its release from keratinocytes. Engagement of intracellular NOD-like receptors (NLRs) by pathogen- or danger-associated molecular

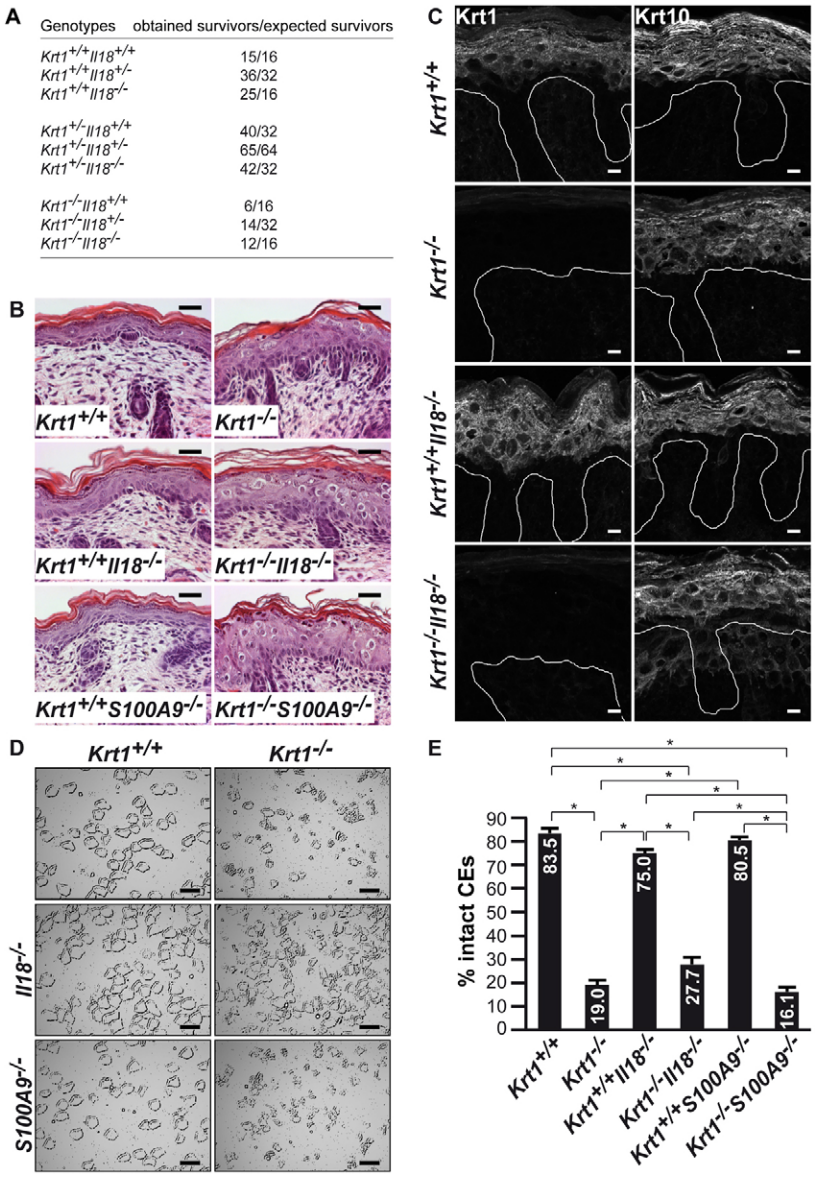

Fig. 6. Genetic rescue of *Krt1*$^{-/-}$ by *Il18*-deficient mice. (**A**) Distribution of 4- to 6-week-old *Krt1*/*Il18* genotypes derived from intercrosses of *Krt1*$^{+/-}$/*Il18*$^{+/-}$ mice. Indicated is the number of animals (obtained survivors/expected survivors according to the Mendelian frequency) of the indicated genotype out of a total of 255 4- to 6-week-old offspring. 37% of *Krt1*$^{+/-}$/*Il18*$^{+/-}$ offspring survived. (**B**) Hematoxylin/Eosin-stained full-thickness back skin sections from *Krt1*$^{+/+}$, *Krt1*$^{-/-}$, *Krt1*$^{+/+}$*Il18*$^{-/-}$, *Krt1*$^{-/-}$*Il18*$^{-/-}$, *Krt1*$^{+/+}$*S100A9*$^{-/-}$ and *Krt1*$^{-/-}$*S100A9*$^{-/-}$ pups at P0. Scale bars: 20 µm. (**C**) Immunofluorescence staining of full-thickness back skin sections from *Krt1*$^{+/+}$, *Krt1*$^{-/-}$, *Krt1*$^{+/+}$*Il18*$^{-/-}$ and *Krt1*$^{-/-}$*Il18*$^{-/-}$ pups at P0 with antibodies against Krt1 and Krt10. The solid line indicates the basement membrane. Scale bars: 10 µm. (**D**) Gross morphology of CEs from *Krt1*$^{+/+}$, *Krt1*$^{-/-}$, *Krt1*$^{+/+}$*Il18*$^{-/-}$, *Krt1*$^{-/-}$*Il18*$^{-/-}$, *Krt1*$^{+/+}$*S100A9*$^{-/-}$ and *Krt1*$^{-/-}$*S100A9*$^{-/-}$ skin at P0. Low differential interference contrast images of CEs were visualized using an artwork filter in Adobe Illustrator CS5.1. Scale bars: 100 µm. (**E**) Quantitative analysis of intact versus fragile CEs at P0 from three mice per indicated genotype. Values are means ± s.e.m. *P<0.05.

pattern molecules activates inflammasomes and caspase-1, which cleaves IL-18 into its active form (Davis et al., 2011; Schroder and Tschopp, 2010; Strowig et al., 2012). Remarkably, NLRP3 (nucleotide-binding-domain, leucine-rich repeat-containing protein) was localized in a keratin-dependent manner in mouse keratinocytes. In contrast to control keratinocytes, NLPR3 distribution appeared more diffuse in keratinocytes in which we had depleted the entire keratin family (Seltmann et al., 2012; Vijayaraj et al., 2009), suggesting a contribution of keratins to the regulation of inflammasome activity (Fig. 7C). We analyzed whether IL-18 processing occurs in a KRT1-dependent manner in human keratinocytes that are known to express higher amounts of KRT1 compared to murine cells upon differentiation (Feldmeyer et al., 2010). Unstimulated human keratinocytes produce significant amounts of proIL-18 but do not release mature IL-18 (Fig. 7A). Upon UVB irradiation, known to increase inflammasome activity and IL-1β release from keratinocytes (Feldmeyer et al., 2007), mature IL-18 was released into the supernatant. Using two caspase-1 inhibitors, IL-18 release could be blocked (Fig. 7A). This demonstrated functionality of the cell system. A knockdown of KRT1 in differentiated human primary keratinocytes resulted in secretion of cleaved IL-18, whereas a simultaneous knockdown of caspase-1 blocked the release of this cytokine (Fig. 7B). This highlighted an important role of KRT1 in inflammasome activation. Thus, Krt1, in contrast to its heterodimer partner Krt10, has unique functions in the maintenance of the cornified envelope, barrier formation and in restraining IL-18 release from keratinocytes. Both Krt1 and Krt10 share an important function in the maintenance of epidermal integrity (Table 1) (Wallace et al., 2012).

Discussion

The epidermal barrier is formed by keratinocytes contributing tight junctions and the cornified envelope, and by Langerhans cells providing immune functions (Simpson et al., 2011). Barrier dysfunction and cutaneous sensitization can give rise to chronic inflammatory disorders including AE and psoriasis. Although both cell types are crucial for barrier functionality, the

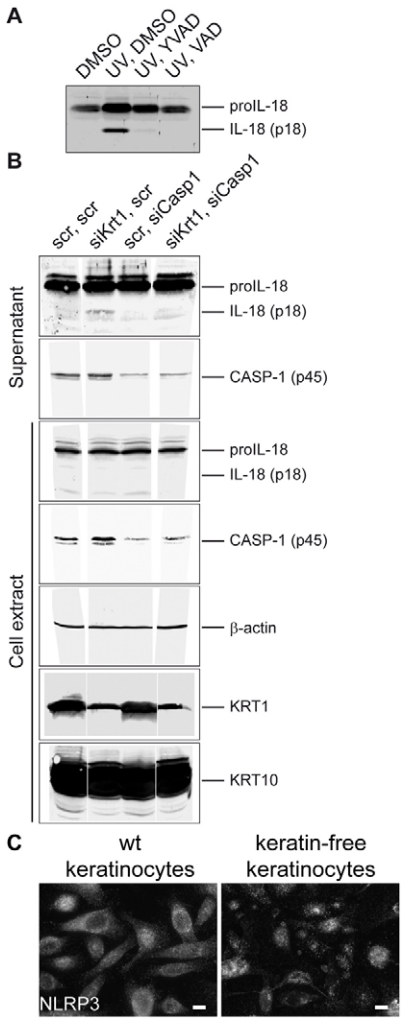

Fig. 7. Knockdown of *KRT1* expression induces caspase-1-dependent secretion of IL-18 in terminally differentiated primary human keratinocytes. (**A**) UVB irradiation of primary human keratinocytes mediates IL-18 secretion. Immunoblot analysis of cell culture supernatants (acetone concentrated) from primary human keratinocytes irradiated with 50 mJ/cm^2 or mock-treated in the presence or absence of the caspase-1 inhibitor YVAD (20 μM) or the pan-caspase inhibitor VAD (10 μM). (**B**) Immunoblot analysis of IL-18, caspase-1 (CASP-1), KRT1 and KRT10 in cell extracts and tissue culture supernatants concentrated by acetone precipitation from differentiated primary human keratinocytes after siRNA knockdown of *Krt1* (siKrt1) and casapse-1 (siCasp1). Scr, scrambled siRNA control. (**C**) Immunofluorescence staining for NLRP3 in wild-type and keratin-cytoskeleton-free primary murine keratinocytes. Scale bars: 10 μm.

significance of epithelial keratinocytes in acute and chronic immune disorders has long been disputed. The recent discovery of filaggrin mutations as an underlying cause of AE has highlighted a major role of keratinocytes in shaping immune responses following barrier disruption and secretion of cytokines including IL-18, IL-33 and TSLP (Haraldsen et al., 2009; Wittmann et al., 2009; Ziegler and Artis, 2010). These seminal findings raise the issue of whether additional keratinocyte-resident proteins contribute to barrier defects and immune disorders through analogous mechanisms.

Until recently, keratins were predominantly regarded as intracellular scaffolds protecting epithelia against mechanical insults, in apparent agreement with phenotypes observed in epidermal keratinopathies (Arin et al., 2010; Arin et al., 2011; Chamcheu et al., 2011; Kim and Coulombe, 2007; Magin et al., 2007). Here, we show for the first time that Krt1, a member of the keratin family of cytoskeleton proteins, plays a major role in epidermal barrier formation and in restricting IL-18 release from keratinocytes, in addition to its role in preserving cell integrity upon elevated mechanical stress. Most importantly, cornified envelope defects, transcriptional upregulation and release of distinct cytokines manifest prenatally upon loss of Krt1, underlining its primary involvement. The specificity of Krt1 is further supported by the very mild phenotype of mice lacking Krt10, its heterodimer partner (Reichelt et al., 2001). As one might predict, combined deletion of *Krt1* and *Krt10* was accompanied by skin fragility more severe than with single gene knockouts (Wallace et al., 2012). In the absence of a side-by side analysis of both mice we speculate that the apparently more severe phenotype of *Krt1/10*$^{-/-}$ compared with *Krt1*$^{-/-}$ is connected to the presence of cytoplasmic Krt10 aggregates in the latter. The limited extent of cell fragility in all three mouse models and the notion that Krt1, but not Krt10, is covalently cross-linked to the CE (Candi et al., 1998) together with our data underscore unique Krt1 functions (see also Table 1).

The prenatal upregulation of IL-18 that occurred at transcriptional and posttranscriptional levels, together with data showing KRT1- and caspase-1-dependent IL-18 release from cultured keratinocytes place Krt1 upstream of IL-18. The importance of IL-18 in this setting is underscored by the partial pharmacological and genetic rescue of the Krt1 phenotype. Collectively, these data suggest a link between components of the epithelial cytoskeleton and inflammasome activation which might contribute to immune responses shifted from a Th1 to a Th2 profile (Kou et al., 2012; Wittmann et al., 2009). In support of this, absence of Krt17 was reported to attenuate inflammation in models of acute dermatitis, characterized by a change in inflammatory cytokines from a Th1- and Th17- to a Th2-dominated inflammatory response (Depianto et al., 2010). More recently, antimicrobial activity of fragments of Krt6A in corneal keratinocyte extracts was reported (Tam et al., 2012). Given the slightly elevated fragility of Krt1/IL-18$^{-/-}$ epidermis, such an activity, if conserved in mouse epidermal keratinocytes, might contribute to the absence of strong inflammation in surviving animals.

The inflammatory signature in *Krt1*$^{-/-}$ mice bears similarity to AE, linked to mutations in the keratin-associated protein filaggrin (Brown and McLean, 2012). The similarity of cytokine profiles and of commonly regulated pathways in *Krt1*$^{-/-}$ mice and AE patients raise the issue of whether Krt1 acts through filaggrin-dependent mechanisms. We find that the absence of Krt1 does not affect filaggrin processing (supplementary material Fig. S2B). Furthermore, elevation of pro-inflammatory cytokines in filaggrin-related AE represents a late event, possibly resulting from a defective barrier and the responding immune system (Brown and McLean, 2012; Kezic et al., 2012; Kou et al., 2012). In contrast to prediction, deletion of filaggrin in mice does not affect survival or cause an elevated trans-epidermal water loss, but results in enhanced responses in contact hypersensitivity (Kawasaki et al., 2012). The unexpectedly mild phenotype arising from complete loss of filaggrin leads to questions about the involvement of KRT1. In a wider context, our data raise the issue of whether conditions in which KRT1 is mutated (e.g. epidermolytic ichthyosis) or downregulated (e.g. squamous cell carcinoma, cutaneous wound healing and HPV infections) (Arin

Table 1. Comparison of major pathological alterations in Krt1, Krt10, Krt1/10 and Krt17 knockout mice

Observation	K1	K10	K1/10	K17
Major phenotype	Inflammation, mild skin fragility	Hyperkeratosis	Severe skin fragility	Alopecia, inflammation
Lethality	P0	None	P0	None
Epid. fragil.	Mild	None	Severe	
Hyperkeratosis	Very mild	Strong	Very mild	
TNFα-dependent alopecia	−	−	−	+
Hair shaft anomalies	−	−	−	+
TEWL	2× ↑	Unalt.	Not done	Not done
Corn. envelope	17% intact	55% intact	40% intact	Not done
Involucrin	Unalt.	−	Reduced	Not done
Loricrin	Unalt.	−	Reduced	Not done
Filaggrin	Unalt.	Unalt.	Unalt.	Not done
Repetin	Elevated	Not done	Not done	Not done
Proliferation	Unalt.	Unalt.	Unalt.	Not done
Compensatory keratin expression	K5/14 ↑ suprabasally K6/16/17 ↑ suprabasally	K5/14 ↑ suprabasally K6/16/17 ↑ suprabasally	− K6 ↑ suprab., K16,K17 not done	K16 ↑ K14 ↑ in sweat glands
K1/K14 filaments	−	+	−	−
K5 or K6/K10 filaments	−	−	−	−
Keratin aggregates	+	−	−	−
Desmosomes	Unalt.	Unalt.	Reduced size	Unalt.
Desmosomal proteins	−	−	Reduced amount	Unalt.
E-cadherin	Unalt.	−	Reduced amount	Unalt.
AMPs	Elevated	−	−	−
IL-18	Elevated	−	−	−
IL-33	Elevated	−	−	−
TSLP	Elevated	−	−	−
S100 A8/9	Elevated	−	−	−
Elevated TNF sensitivity	Not done	Not done	Not done	Yes

Epid. fragil., epidermal fragility; Unalt., unaltered; suprab., suprabasal; ↑, an increase; +, present; −, absent. Data were compiled from knockout mice for Krt1 (this manuscript); Krt10 (Reichelt et al., 2001), Krt1/Krt10 (Wallace et al., 2012), Krt 17 (McGowan et al., 2002; Tong and Coulombe, 2006).

et al., 2011; Depianto et al., 2010; Longworth and Laimins, 2004) carry an inflammatory signature similar to that seen in *Krt1*$^{-/-}$ mice. Our data connect the presence of KRT1 to a keratinocyte-based network that restrains inflammation and, in conjunction with Krt17 (Depianto et al., 2010), provide strong evidence for context-dependent functions of keratin isotypes that extend beyond formation of cytoskeletal scaffolds in epithelia.

Materials and Methods

Mice

Krt1$^{-/-}$ mice were generated by targeted disruption of the *Krt1* gene by homologous recombination in embryonic stem cells (supplementary material Fig. S1B). Hence, exon1, intron 1 and ~415 bp from the 5′ UTR were deleted and replaced with an Hprt-minigene cassette (Reichelt et al., 2001). All mice were from a mixed 129/SvJ×C57BL/6 background. Experiments were performed according to institutional regulations. Offspring from heterozygous intercrosses were genotyped by PCR analysis of tail DNA (supplementary material Table S6 for details). Genotypes of *Krt1*$^{-/-}$ offspring were confirmed by western blot analysis of skin protein extracts with a polyclonal anti-Krt1 rabbit antiserum.

Antibodies

See supplementary material Table S7.

Immunohistochemistry and immunofluorescence

Preparation of tissue samples and immunofluorescence analysis were carried out as described previously (Roth et al., 2009). Horseradish-peroxidase-conjugated secondary antibodies were detected using the Super Sensitive Link-Label IHC Detection System (BioGenex Laboratories, Fremont, CA, USA) with diaminobenzidine (Dako, Hamburg, Germany). Images were acquired at ambient temperature with an Axioplan 2 fluorescence microscope (Carl Zeiss, Jena, Germany) equipped with Zeiss Plan-Apochromat 63×/1.4 and Plan-Neofluar 40×/1.3 oil immersion objectives, and recorded with an AxiocamHR camera (Carl Zeiss, Jena, Germany). Image analysis and processing were performed using the AxioVision 4.6 software (Carl Zeiss, Jena, Germany). Confocal images were recorded on an LSM710 microscope equipped with a Zeiss63×LCI Plan Neofluar objective (Carl Zeiss, Jena Germany). Fluorochromes were sequentially scanned to avoid cross-talk between channels using Pinhole 'airy 1' Zeiss standard settings. Z-stacks of 8–12 consecutive sections were recorded and processed as maximum intensity projections. Image analysis and processing were performed with the Zen software (Carl Zeiss, Jena, Germany). Images were cropped and analyzed in Adobe Photoshop CS4; Adobe Illustrator CS4 was used for figure design.

Western blot analysis

Full-thickness skin samples were lysed in 5× Laemmli buffer and homogenized (Ultra Turrax). Immunoblot analysis was performed as described previously (Löffek et al., 2010).

Preparation of epidermis

Full-thickness mouse skin was floated on 0.5 M ammonium thiocyanate (Sigma-Aldrich, St Louis, MO, USA) as described previously (Reichelt and Magin, 2002) to isolate epidermal sheets.

RNA preparation

Epidermal sheets or full-thickness skin samples were homogenized (Ultra-Turrax) in TRIzol (Life Technologies, Darmstadt, Germany) supplemented with ribonucleoside–vanadyl complexes (New England BioLabs, Ipswich, MA, USA). Total RNA was phenol/chloroform extracted, precipitated, treated with DNaseI (Fermentas Life Science, Leon-Rot, Germany) and purified with the RNeasy MinElute Cleanup kit (Qiagen, Hilden, Germany).

Gene expression profiling

The MouseWG-6v2.0 Expression BeadChip kit (Illumina, Inc., San Diego, CA, USA) was used to probe triplicate $Krt1^{+/+}$ and $Krt1^{-/-}$ samples. Data analysis was based on the R Statistical language (R Development Core Team 2007, 2.8.0) and Beadstudio 3.1.1.0 software. Data were quantile-normalized. A fold-change/*P*-value filter was used to select differentially expressed genes; *P*-values smaller than 0.05, expression changes higher than twofold and a difference between mean intensity signals greater than background were considered statistically significant. The false discovery rate (FDR) of *P*-values was adjusted by the Benjamini–Hochberg method. Heatmaps were generated based on average linkage and the Pearson correlation coefficient, with blue indicating low level, white intermediate and red high levels of gene expression. The gene expression data sets were deposited in the GEO database (GES32951).

Transcriptome data from AE (E-GEOD-12511), psoriasis (E-GEOD-13355), *Krt5* P0 (E-GEOD-7663) and EBS (E-GEOD-28315) were downloaded from the EBI server for the further comparison analysis (Bchetnia et al., 2012; Gudjonsson et al., 2010; Lu et al., 2007; Sääf et al., 2008). For data processing GNU R (www.r-project.org) with the Bioconductor packages (www.bioconductor.org) were used. Data were normalized by RMA algorithms. *Krt1* data were individually analyzed or evaluated in conjunction with the additional transcriptome data sets.

For cross platform and a cross species comparison the transcriptome data sets (A and B) were annotated by gene symbols and normalized by its standard deviation. In the first step of this normalization the gene expression ($y_{i,j}$) of the gene (i) on array (j) in set A was normalized by the following equation:

$$y'_{i,j} = \frac{y_{i,j} - \mu_{setA}}{\sigma_{setA}} \sigma_{setA \cup B} + \mu_{setA \cup B}. \quad (1)$$

Secondly, the cross species adaption was achieved by equalizing the controls of each set by the following equation:

$$y''_{i,j} = y'_{i,j} - \bar{y}'_{i,j \in controlsofsetA} + \bar{y}'_{i,j \in controlsofsetA \cup B}. \quad (2)$$

Gene set enrichment analysis

For the gene set enrichment analysis (GSEA) the Molecular Signatures Database (MSigDB database v3.0, Broad Institute) was used. To minimize the noise the enrichment score of each set was calculated using root square means. *P*-values were calculated using Student's *t*-test. To calculate the similarity of *Krt1* data and the additional expression data sets the minimum difference to the control was used:

$$y'''_i = \mathrm{sgn}\left(\frac{\bar{y}''_{i,A} - \bar{y}''_{i,controle}}{\bar{y}''_{i,B} - \bar{y}''_{i,controle}}\right) MIN\left(\left|\bar{y}''_{i,A} - \bar{y}''_{i,controle}\right|, \left|\bar{y}''_{i,B} - \bar{y}''_{i,controle}\right|\right). \quad (3)$$

Network figures of the enriched pathways were generated using the Cytoscape tool version 2.6.1 (www.cytoscape.org) with the Enrichment Map plug in (Merico et al., 2010). The top 100 enriched pathways with a *P*-value <0.001 were used.

Real-time PCR

cDNA synthesis was carried out using a RevertAid H Minus First Strand cDNA Synthesis kit (Fermentas Life Science, Leon-Rot, Germany). Real-time PCR was performed with a Maxima SYBR Green/ROX qPCR Master Mix (Fermentas Life Science, Leon-Rot, Germany) and run on a Mastercycler ep realplex (Eppendorf, Hamburg, Germany). 18S RNA was used as a reference. Mouse qPCR primer sequences are shown in supplementary material Table S8.

Determination of cytokine concentrations

IL-18 and IL-33 were measured by ELISA (Bender MedSystems, Vienna, Austria; Quantikine, R&D Systems, Minneapolis, MN, USA). Mrp8 and Mrp14 protein levels were determined by ELISA as described previously (Vogl et al., 2007). TSLP protein levels were determined by mouse cytokine antibody array analysis (C series 1000.1; RayBiotech, Inc., Norcross, GA, USA) as described previously (Roth et al., 2009).

Analysis of transepidermal water loss

TEWL was assessed in triplicate readings on the dorsal neck skin of newborn mice using a Tewameter (TM 300, Courage and Khazaka Electronic, Cologne, Germany).

Blocking antibody treatment

Females were injected intraperitoneally at E18.5 with 20 μg anti-IL-18 blocking antibody (clone 93-10C, R&D Systems, Minneapolis, MN, USA) or IgG1 immunoglobulins (R&D Systems, Minneapolis, MN, USA) as control. Newborn pups were treated with 4 μg of antibody or IgG1 at P0 and P1. At P2, mice were killed and analyzed.

Keratinocyte culture and transfection

In human primary keratinocytes (Feldmeyer et al., 2007), differentiation was induced by culture in KBM-2 (Cambrex, East Rutherford, NJ, USA) for 6 days. Keratinocytes were UV-irradiated with 50 mJ/cm^2 (Medisun HF-54, Schulze and Boehm, Bruehl, Germany) in the presence of the synthetic tetrapeptide YVAD (Tyr-Val-Ala-Asp; 20 μM), VAD (valyl-alanyl-aspartyl; 10 μM; Enzo Life Sciences, Lorrach, Germany) or DMSO (vehicle) and harvested after 4 h. For knockdown experiments, 10 nM siRNAs and Interferin (Polyplus transfection, Illkirch, France) were used. Cells and supernatants were harvested after 6 days; total protein from the supernatant was acetone precipitated. Sequence information of siRNAs (Sigma-Aldrich, St. Louis, MO, USA) used is provided in supplementary material Table S9.

Statistical analysis

Statistical significance was determined by unpaired *t*-tests for two groups and analysis of variance tests for more than two groups. The alpha level was set at <0.05. Data were analyzed with Sigma Plot 11.0 and plotted with Excel. All statistical data are shown in supplementary material Table S10.

Acknowledgements

We thank Roland Bornheim for the generation of the $Krt1^{+/-}$ mouse line. We thank B. Fuss and M. Hoch for access to their LSM710.

Funding

This work was partially supported by grants from the Thyssen Foundation [Thyssen 10.02.1.103 to T.M.M. and J. Reichelt]; BONFOR, Deutsche Forschungsgemeinschaft [DFG 1316/9 to T.M.M.]; and the Translational Centre for Regenerative Medicine Leipzig [PtJ-Bio, 0315883 to T.M.M.].

Supplementary material available online at
http://jcs.biologists.org/lookup/suppl/doi:10.1242/jcs.116574/-/DC1

References

Arin, M. J., Grimberg, G., Schumann, H., De Almeida, H., Jr, Chang, Y. R., Tadini, G., Kohlhase, J., Krieg, T., Bruckner-Tuderman, L. and Has, C. (2010). Identification of novel and known KRT5 and KRT14 mutations in 53 patients with epidermolysis bullosa simplex: correlation between genotype and phenotype. *Br. J. Dermatol.* **162**, 1365-1369.

Arin, M. J., Oji, V., Emmert, S., Hausser, I., Traupe, H., Krieg, T. and Grimberg, G. (2011). Expanding the keratin mutation database: novel and recurrent mutations and genotype-phenotype correlations in 28 patients with epidermolytic ichthyosis. *Br. J. Dermatol.* **164**, 442-447.

Barnes, K. C. (2010). An update on the genetics of atopic dermatitis: scratching the surface in 2009. *J. Allergy Clin. Immunol.* **125**, 16-29.

Bchetnia, M., Tremblay, M. L., Leclerc, G., Dupérée, A., Powell, J., McCuaig, C., Morin, C., Legendre-Guillemin, V. and Laprise, C. (2012). Expression signature of epidermolysis bullosa simplex. *Hum. Genet.* **131**, 393-406.

Brown, S. J. and McLean, W. H. (2012). One remarkable molecule: filaggrin. *J. Invest. Dermatol.* **132**, 751-762.

Candi, E., Tarcsa, E., Digiovanna, J. J., Compton, J. G., Elias, P. M., Marekov, L. N. and Steinert, P. M. (1998). A highly conserved lysine residue on the head domain of type II keratins is essential for the attachment of keratin intermediate filaments to the cornified cell envelope through isopeptide crosslinking by transglutaminases. *Proc. Natl. Acad. Sci. USA* **95**, 2067-2072.

Candi, E., Schmidt, R. and Melino, G. (2005). The cornified envelope: a model of cell death in the skin. *Nat. Rev. Mol. Cell Biol.* **6**, 328-340.

Chamcheu, J. C., Siddiqui, I. A., Syed, D. N., Adhami, V. M., Liovic, M. and Mukhtar, H. (2011). Keratin gene mutations in disorders of human skin and its appendages. *Arch. Biochem. Biophys.* **508**, 123-137.

Davis, B. K., Wen, H. and Ting, J. P. (2011). The inflammasome NLRs in immunity, inflammation, and associated diseases. *Annu. Rev. Immunol.* **29**, 707-735.

Depianto, D., Kerns, M. L., Dlugosz, A. A. and Coulombe, P. A. (2010). Keratin 17 promotes epithelial proliferation and tumor growth by polarizing the immune response in skin. *Nat. Genet.* **42**, 910-914.

Dinarello, C. A. (2009). Immunological and inflammatory functions of the interleukin-1 family. *Annu. Rev. Immunol.* **27**, 519-550.

Eckert, R. L., Broome, A. M., Ruse, M., Robinson, N., Ryan, D. and Lee, K. (2004). S100 proteins in the epidermis. *J. Invest. Dermatol.* **123**, 23-33.

Ehrchen, J. M., Sunderkötter, C., Foell, D., Vogl, T. and Roth, J. (2009). The endogenous Toll-like receptor 4 agonist S100A8/S100A9 (calprotectin) as innate amplifier of infection, autoimmunity, and cancer. *J. Leukoc. Biol.* **86**, 557-566.

Feldmeyer, L., Keller, M., Niklaus, G., Hohl, D., Werner, S. and Beer, H. D. (2007). The inflammasome mediates UVB-induced activation and secretion of interleukin-1beta by keratinocytes. *Curr. Biol.* **17**, 1140-1145.

Feldmeyer, L., Werner, S., French, L. E. and Beer, H. D. (2010). Interleukin-1, inflammasomes and the skin. *Eur. J. Cell Biol.* **89**, 638-644.

Gudjonsson, J. E., Ding, J., Li, X., Nair, R. P., Tejasvi, T., Qin, Z. S., Ghosh, D., Aphale, A., Gumucio, D. L., Voorhees, J. J. et al. (2009). Global gene expression analysis reveals evidence for decreased lipid biosynthesis and increased innate immunity in uninvolved psoriatic skin. *J. Invest. Dermatol.* **129**, 2795-2804.

Gudjonsson, J. E., Ding, J., Johnston, A., Tejasvi, T., Guzman, A. M., Nair, R. P., Voorhees, J. J., Abecasis, G. R. and Elder, J. T. (2010). Assessment of the psoriatic transcriptome in a large sample: additional regulated genes and comparisons with *in vitro* models. *J. Invest. Dermatol.* **130**, 1829-1840.

Haraldsen, G., Balogh, J., Pollheimer, J., Sponheim, J. and Küchler, A. M. (2009). Interleukin-33 - cytokine of dual function or novel alarmin? *Trends Immunol.* **30**, 227-233.

Hochholzer, P., Lipford, G. B., Wagner, H., Pfeffer, K. and Heeg, K. (2000). Role of interleukin-18 (IL-18) during lethal shock: decreased lipopolysaccharide sensitivity but normal superantigen reaction in IL-18-deficient mice. *Infect. Immun.* **68**, 3502-3508.

Kambe, N., Nakamura, Y., Saito, M. and Nishikomori, R. (2010). The inflammasome, an innate immunity guardian, participates in skin urticarial reactions and contact hypersensitivity. *Allergol. Int.* **59**, 105-113.

Kawasaki, H., Nagao, K., Kubo, A., Hata, T., Shimizu, A., Mizuno, H., Yamada, T. and Amagai, M. (2012). Altered stratum corneum barrier and enhanced percutaneous immune responses in filaggrin-null mice. *J. Allergy Clin. Immunol.* **129**, 1538-1546.

Keller, A., Backes, C., Al-Awadhi, M., Gerasch, A., Küntzer, J., Kohlbacher, O., Kaufmann, M. and Lenhof, H. P. (2008). GeneTrailExpress: a web-based pipeline for the statistical evaluation of microarray experiments. *BMC Bioinformatics* **9**, 552.

Kezic, S., O'Regan, G. M., Lutter, R., Jakasa, I., Koster, E. S., Saunders, S., Caspers, P., Kemperman, P. M., Puppels, G. J., Sandilands, A. et al. (2012). Filaggrin loss-of-function mutations are associated with enhanced expression of IL-1 cytokines in the stratum corneum of patients with atopic dermatitis and in a murine model of filaggrin deficiency. *J. Allergy Clin. Immunol.* **129**, 1031-1039.

Kim, S. and Coulombe, P. A. (2007). Intermediate filament scaffolds fulfill mechanical, organizational, and signaling functions in the cytoplasm. *Genes Dev.* **21**, 1581-1597.

Konishi, H., Tsutsui, H., Murakami, T., Yumikura-Futatsugi, S., Yamanaka, K., Tanaka, M., Iwakura, Y., Suzuki, N., Takeda, K., Akira, S. et al. (2002). IL-18 contributes to the spontaneous development of atopic dermatitis-like inflammatory skin lesion independently of IgE/stat6 under specific pathogen-free conditions. *Proc. Natl. Acad. Sci. USA* **99**, 11340-11345.

Kou, K., Aihara, M., Matsunaga, T., Chen, H., Taguri, M., Morita, S., Fujita, H., Yamaguchi, Y., Kambara, T. and Ikezawa, Z. (2012). Association of serum interleukin-18 and other biomarkers with disease severity in adults with atopic dermatitis. *Arch. Dermatol. Res.* **304**, 305-312.

Kubo, A., Nagao, K. and Amagai, M. (2012). Epidermal barrier dysfunction and cutaneous sensitization in atopic diseases. *J. Clin. Invest.* **122**, 440-447.

Lane, E. B. and McLean, W. H. (2004). Keratins and skin disorders. *J. Pathol.* **204**, 355-366.

Löffek, S., Wöll, S., Höhfeld, J., Leube, R. E., Has, C., Bruckner-Tuderman, L. and Magin, T. M. (2010). The ubiquitin ligase CHIP/STUB1 targets mutant keratins for degradation. *Hum. Mutat.* **31**, 466-476.

Longworth, M. S. and Laimins, L. A. (2004). Pathogenesis of human papillomaviruses in differentiating epithelia. *Microbiol. Mol. Biol. Rev.* **68**, 362-372.

Lu, H., Chen, J., Planko, L., Zigrino, P., Klein-Hitpass, L. and Magin, T. M. (2007). Induction of inflammatory cytokines by a keratin mutation and their repression by a small molecule in a mouse model for EBS. *J. Invest. Dermatol.* **127**, 2781-2789.

Magin, T. M., Vijayaraj, P. and Leube, R. E. (2007). Structural and regulatory functions of keratins. *Exp. Cell Res.* **313**, 2021-2032.

Manitz, M. P., Horst, B., Seeliger, S., Strey, A., Skryabin, B. V., Gunzer, M., Frings, W., Schönlau, F., Roth, J., Sorg, C. et al. (2003). Loss of S100A9 (MRP14) results in reduced interleukin-8-induced CD11b surface expression, a polarized microfilament system, and diminished responsiveness to chemoattractants *in vitro*. *Mol. Cell. Biol.* **23**, 1034-1043.

McGowan, K. M., Tong, X., Colucci-Guyon, E., Langa, F., Babinet, C. and Coulombe, P. A. (2002). Keratin 17 null mice exhibit age- and strain-dependent alopecia. *Genes Dev.* **16**, 1412-1422.

Merico, D., Isserlin, R., Stueker, O., Emili, A. and Bader, G. D. (2010). Enrichment map: a network-based method for gene-set enrichment visualization and interpretation. *PLoS ONE* **5**, e13984.

Nestle, F. O., Di Meglio, P., Qin, J. Z. and Nickoloff, B. J. (2009). Skin immune sentinels in health and disease. *Nat. Rev. Immunol.* **9**, 679-691.

Oji, V., Tadini, G., Akiyama, M., Blanchet Bardon, C., Bodemer, C., Bourrat, E., Coudiere, P., DiGiovanna, J. J., Elias, P., Fischer, J. et al. (2010). Revised nomenclature and classification of inherited ichthyoses: results of the First Ichthyosis Consensus Conference in Sorèze 2009. *J. Am. Acad. Dermatol.* **63**, 607-641.

Quigley, D. A., To, M. D., Pérez-Losada, J., Pelorosso, F. G., Mao, J. H., Nagase, H., Ginzinger, D. G. and Balmain, A. (2009). Genetic architecture of mouse skin inflammation and tumour susceptibility. *Nature* **458**, 505-508.

Reichelt, J. and Magin, T. M. (2002). Hyperproliferation, induction of c-Myc and 14-3-3sigma, but no cell fragility in keratin-10-null mice. *J. Cell Sci.* **115**, 2639-2650.

Reichelt, J., Büssow, H., Grund, C. and Magin, T. M. (2001). Formation of a normal epidermis supported by increased stability of keratins 5 and 14 in keratin 10 null mice. *Mol. Biol. Cell* **12**, 1557-1568.

Roth, W., Reuter, U., Wohlenberg, C., Bruckner-Tuderman, L. and Magin, T. M. (2009). Cytokines as genetic modifiers in K5-/- mice and in human epidermolysis bullosa simplex. *Hum. Mutat.* **30**, 832-841.

Sääf, A. M., Tengvall-Linder, M., Chang, H. Y., Adler, A. S., Wahlgren, C. F., Scheynius, A., Nordenskjöld, M. and Bradley, M. (2008). Global expression profiling in atopic eczema reveals reciprocal expression of inflammatory and lipid genes. *PLoS ONE* **3**, e4017.

Schmuth, M., Yosipovitch, G., Williams, M. L., Weber, F., Hintner, H., Ortiz-Urda, S., Rappersberger, K., Crumrine, D., Feingold, K. R. and Elias, P. M. (2001). Pathogenesis of the permeability barrier abnormality in epidermolytic hyperkeratosis. *J. Invest. Dermatol.* **117**, 837-847.

Schroder, K. and Tschopp, J. (2010). The inflammasomes. *Cell* **140**, 821-832.

Schweizer, J., Bowden, P. E., Coulombe, P. A., Langbein, L., Lane, E. B., Magin, T. M., Maltais, L., Omary, M. B., Parry, D. A., Rogers, M. A. et al. (2006). New consensus nomenclature for mammalian keratins. *J. Cell Biol.* **174**, 169-174.

Segre, J. A. (2006). Epidermal barrier formation and recovery in skin disorders. *J. Clin. Invest.* **116**, 1150-1158.

Segre, J. A., Bauer, C. and Fuchs, E. (1999). Klf4 is a transcription factor required for establishing the barrier function of the skin. *Nat. Genet.* **22**, 356-400.

Seltmann, K., Roth, W., Kröger, C., Loschke, F., Lederer, M., Hüttelmaier, S. and Magin, T. M. (2012). Keratins mediate localization of hemidesmosomes and repress cell motility. *J. Invest. Dermatol*. [Epub ahead of print] doi:10.1038/jid.2012.256.

Simpson, C. L., Patel, D. M. and Green, K. J. (2011). Deconstructing the skin: cytoarchitectural determinants of epidermal morphogenesis. *Nat. Rev. Mol. Cell Biol.* **12**, 565-580.

Strowig, T., Henao-Mejia, J., Elinav, E. and Flavell, R. (2012). Inflammasomes in health and disease. *Nature* **481**, 278-286.

Suárez-Fariñas, M., Lowes, M. A., Zaba, L. C. and Krueger, J. G. (2010). Evaluation of the psoriasis transcriptome across different studies by gene set enrichment analysis (GSEA). *PLoS ONE* **5**, e10247.

Suárez-Fariñas, M., Tintle, S. J., Shemer, A., Chiricozzi, A., Nograles, K., Cardinale, I., Duan, S., Bowcock, A. M., Krueger, J. G. and Guttman-Yassky, E. (2011). Nonlesional atopic dermatitis skin is characterized by broad terminal differentiation defects and variable immune abnormalities. *J. Allergy Clin. Immunol.* **127**, 954-964.

Tam, C., Mun, J. J., Evans, D. J. and Fleiszig, S. M. (2012). Cytokeratins mediate epithelial innate defense through their antimicrobial properties. *J. Clin. Invest.* **122**, 3665-3677.

Tong, X. and Coulombe, P. A. (2006). Keratin 17 modulates hair follicle cycling in a TNFalpha-dependent fashion. *Genes Dev.* **20**, 1353-1364.

Vijayaraj, P., Kröger, C., Reuter, U., Windoffer, R., Leube, R. E. and Magin, T. M. (2009). Keratins regulate protein biosynthesis through localization of GLUT1 and -3 upstream of AMP kinase and Raptor. *J. Cell Biol.* **187**, 175-184.

Vogl, T., Tenbrock, K., Ludwig, S., Leukert, N., Ehrhardt, C., van Zoelen, M. A., Nacken, W., Foell, D., van der Poll, T., Sorg, C. et al. (2007). Mrp8 and Mrp14 are endogenous activators of Toll-like receptor 4, promoting lethal, endotoxin-induced shock. *Nat. Med.* **13**, 1042-1049.

Wallace, L., Roberts-Thompson, L. and Reichelt, J. (2012). Deletion of K1/K10 does not impair epidermal stratification but affects desmosomal structure and nuclear integrity. *J. Cell Sci.* **125**, 1750-1758.

Wittmann, M., Macdonald, A. and Renne, J. (2009). IL-18 and skin inflammation. *Autoimmun. Rev.* **9**, 45-48.

Ziegler, S. F. and Artis, D. (2010). Sensing the outside world: TSLP regulates barrier immunity. *Nat. Immunol.* **11**, 289-293.

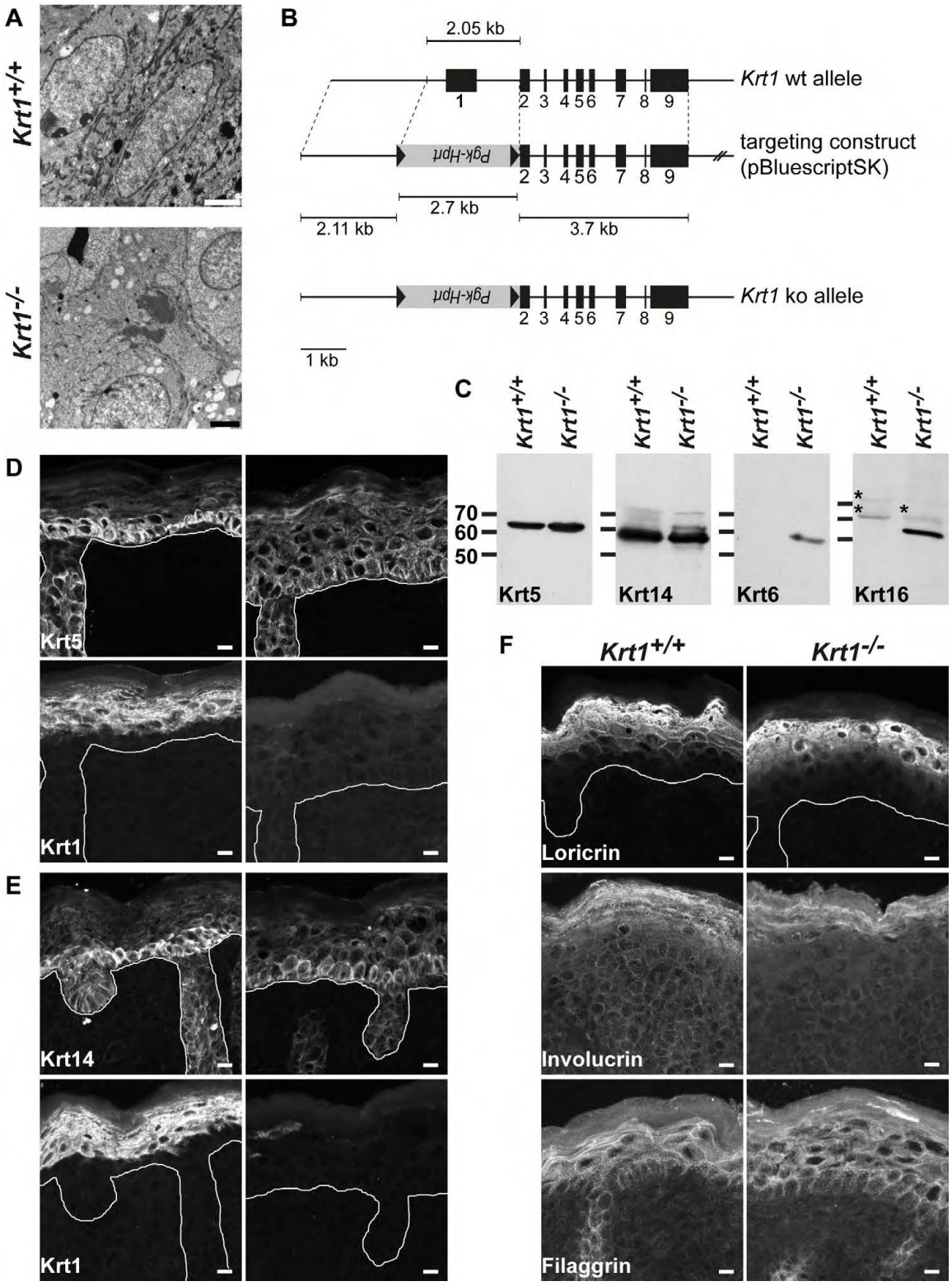

Fig. S1. *Krt1*$^{-/-}$ mice show normal epidermal morphology and unaltered expression of differentiation markers. (**A**) Electron micrographs of the suprabasal epidermis of *Krt1*$^{+/+}$ and *Krt1*$^{-/-}$ pups at P0. Scale bars, 2 µm for *Krt1*$^{+/+}$ and 200 nm for *Krt1*$^{-/-}$. (**B**) *Krt1* knockout strategy. *Krt1*$^{-/-}$ mice were generated by targeted disruption of *Krt1* gene *via* homologous recombination in embryonic stem cells. In the targeting construct exon1, intron 1 and ~415 bp from the 5' UTR were deleted and replaced by an Hprt-minigene cassette. The Hprt minigene cassette is flanked at the 5' end by a 2.1 kb and at the 3' end by a 3.7 kb genomic region homologous to the *Krt1* genomic locus. (**C**) Immunoblot analysis of indicated keratin expression in total skin extracts from *Krt1*$^{+/+}$ and *Krt1*$^{-/-}$ pups at P0. Asterisks mark non-specific cross-reactivity of the antibody. (**D** and **E**) Double immunofluorescence staining of full-thickness back skin sections from *Krt1*$^{+/+}$ and *Krt1*$^{-/-}$ pups at P0 with antibodies against Krt5 and Krt1 (**D**) or against Krt14 and Krt1 (**E**). Scale bars, 10 µm. Solid line indicates basement membrane. (**F**) Immunofluorescence analyses of the epidermal differentiation markers loricrin, involucrin and filaggrin at P0. Scale bars, 10 µm. Solid line indicates basement membrane.

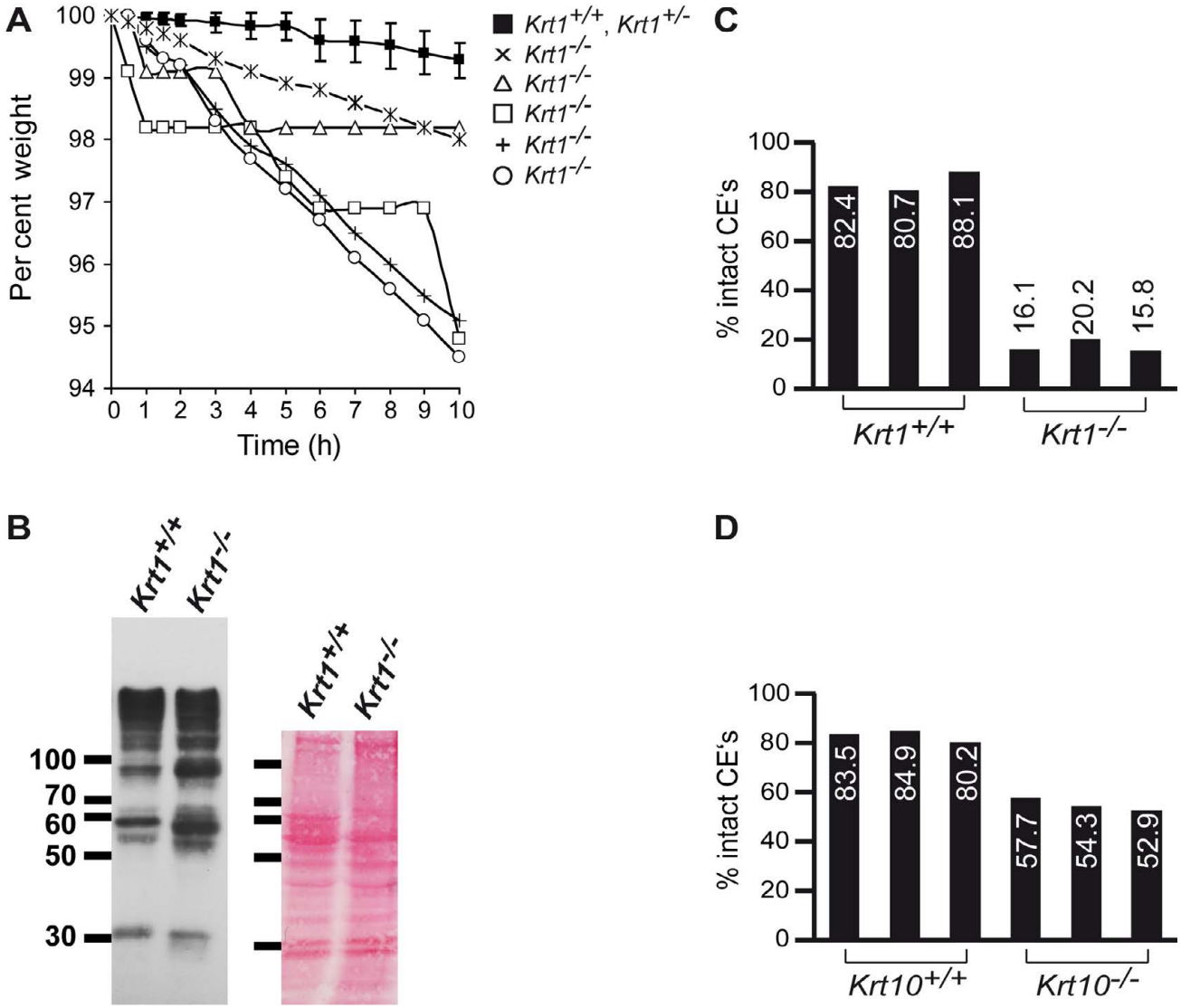

Fig. S2. Newborn *Krt1*$^{-/-}$ mice show a defective epidermal barrier but normal filaggrin protein expression and processing. (**A**) Time course of dehydration measurement indicating a postnatal weight loss in newborn *Krt1*$^{-/-}$ pups. Values are percentages ± s.d. of initial body weights (1.061–1.480 g); in wild-type, no differences in weight loss between *Krt1*$^{+/+}$ and *Krt*$^{+/-}$ pups were observed. (**B**) Immunoblot analysis of filaggrin expression in total skin extracts from *Krt1*$^{+/+}$ and *Krt1*$^{-/-}$ pups at P0. Equal loading was assessed by Ponceau S staining of the blotted protein on nitrocellulose membranes. (**C**) Relative percentages of intact CEs from three individual *Krt1*$^{+/+}$ and *Krt1*$^{-/-}$ newborn pups (P0); CEs were counted with a hemocytometer (see **Figure 3B**). (**D**) Relative percentages of intact CEs from three *Krt10*$^{+/+}$ and three *Krt10*$^{-/-}$ newborn pups (P0); CEs were counted with a hemocytometer (see **Figure 3C**).

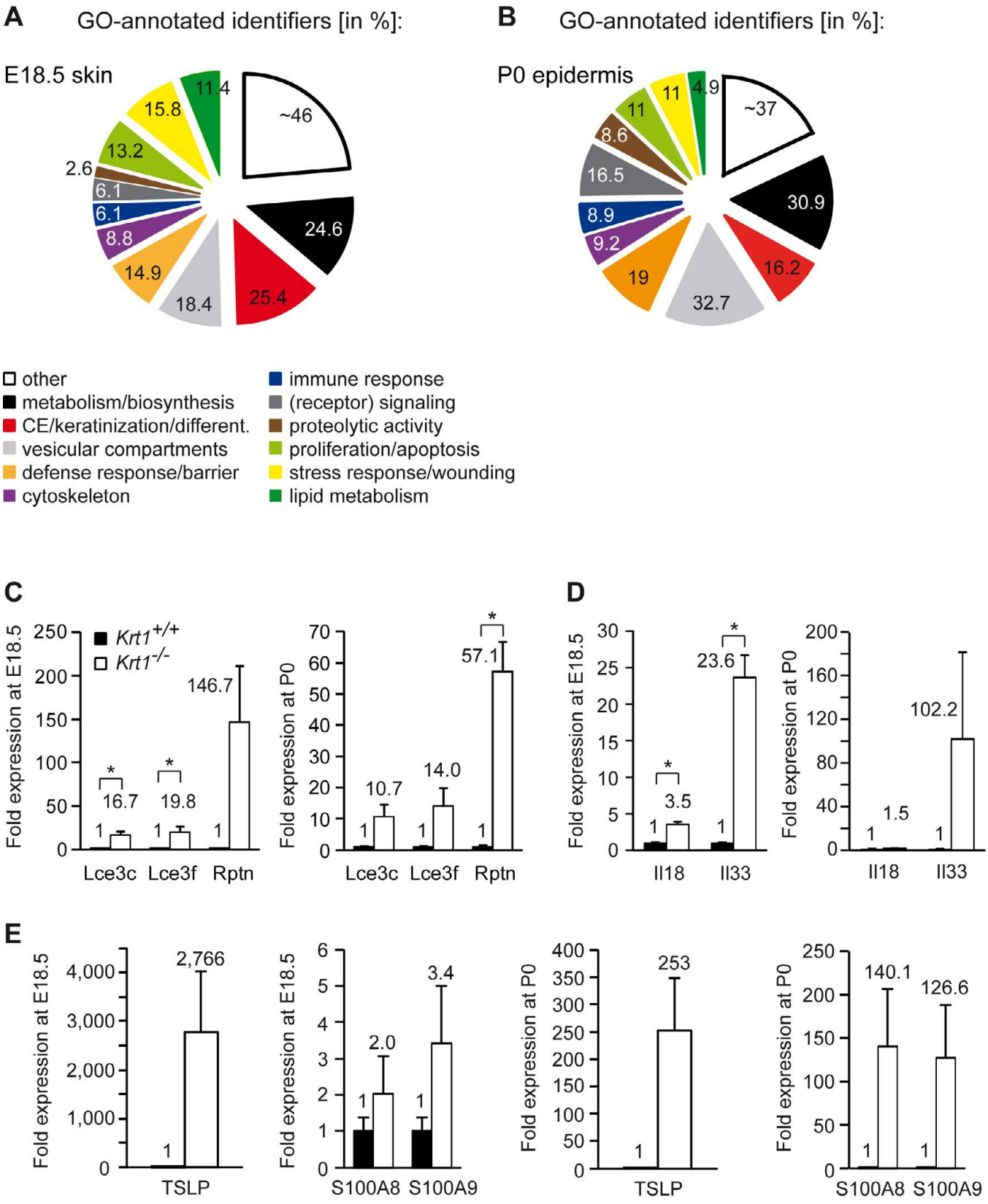

Fig. S3. Functional defects in the epidermal barrier and activation of innate immune responses establish prenatally. (**A** and **B**) Pie charts of up-regulated genes in *Krt1*$^{-/-}$ versus *Krt1*$^{+/+}$ epidermis at E18.5 (**A**) and at P0 (**B**). Genes were classified by Gene Ontology and grouped by function. (**C**) Quantitative RT-PCR analysis of selected CE genes in P0 epidermis and E18.5 skin. Values are mean ± SEM of three samples per genotype measured in duplicate. **P*<0.05. (**D** and **E**) Quantitative RT-PCR (qPCR) analysis of selected candidate genes from P0 epidermis and E18.5 skin confirmed the upregulation of immune response genes in *Krt1*$^{-/-}$ skin. (**D**) qPCR of Il18 and Il33. (**E**) qPCR of TSLP, S100A8, and S100A9. Values are mean ± SEM of three samples per genotype measured in duplicate. **P*<0.05.

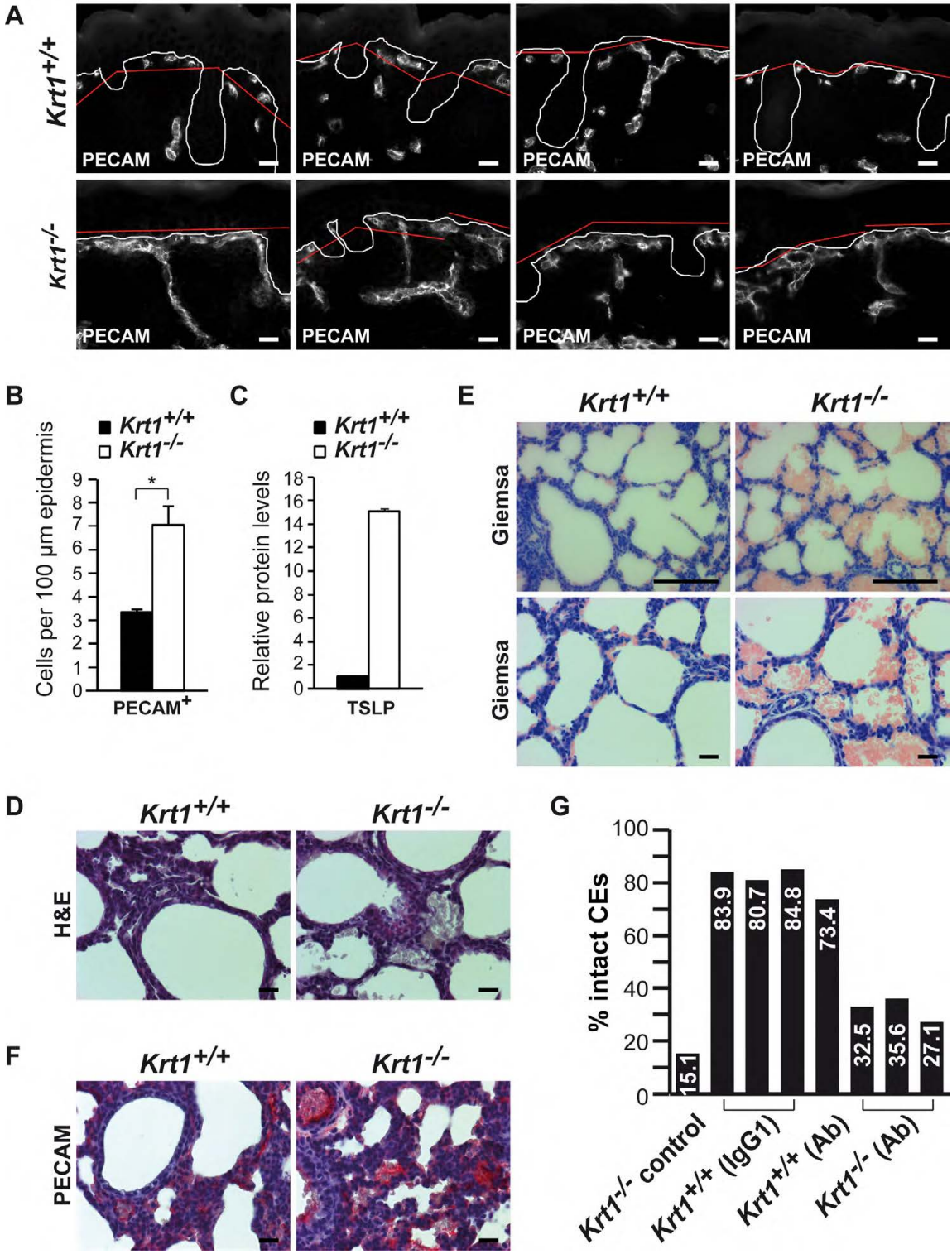

Fig. S4. Systemic defects mediated by loss of Krt1. (**A**) Immunofluorescence staining of full-thickness back skin sections from *Krt1*$^{+/+}$ and *Krt1*$^{-/-}$ newborn pups at P0 with antibodies against PECAM to visualize microvessels in skin. White solid line indicates basement membrane. Red solid line represents the lengthwise measurement of the epidermal segment for quantification. Scale bar, 20 µm. (**B**) Quantitative analysis of PECAM-positive cells to assess the extent of skin vascularization. Five to six microscopic fields (**A**) per genotype (n=3) were analyzed for PECAM staining. (**C**) Cytokine antibody array analysis of relative TSLP protein level in tissue extracts from pooled *Krt1*$^{+/+}$ and *Krt1*$^{-/-}$ epidermis (n=6). Shown is one representative result of two independent experiments. (**D-F**) Histological analysis of newborn lung (P0) tissue stained with (**D**) hematoxylin & eosin, (**E**) Giemsa, and (**F**) anti-PECAM antibodies. Scale bar, 20 µm. Scale bar upper panel Giemsa stain, 100 µm. **(G)** IL-18 blocking antibodies partially rescue the phenotype of *Krt1*$^{-/-}$ neonates. Intact *versus* fragile CEs in treated and untreated *Krt1*$^{+/+}$ and *Krt*$^{-/-}$ mice at P2. CEs were counted with a hemocytometer (see **Figure 5F** and **G**). Relative percentages of intact CEs in individual *Krt1*$^{+/+}$ and *Krt*$^{-/-}$ mice are given at P2.

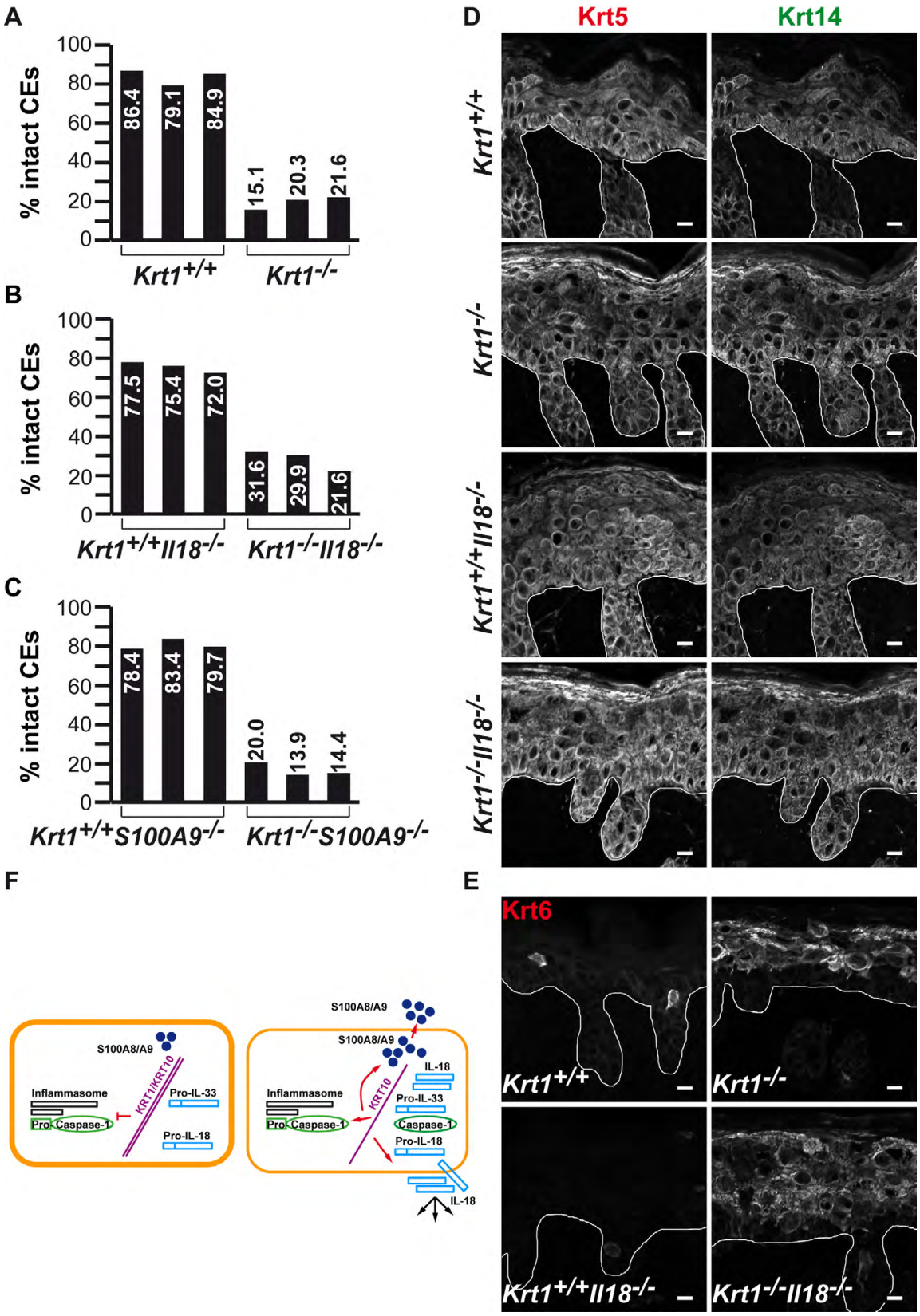

Fig. S5. The phenotype of *Krt1*$^{-/-}$ mice can be partially rescued in an *Il18*-deficient, but not in a *S100A9*-deficient genetic background. (**A-C**) Relative percentages of intact CEs are shown from individual newborn pups (P0) of indicated genotypes; CEs were counted with a hemocytometer (see Figure 6D and E). (**D**) Double immunofluorescence staining of full-thickness back skin sections from newborn pups at P0 of the indicated genotypes with antibodies against Krt5 and Krt14. Scale bars, 10 µm. Solid line indicates basement membrane. (**E**) Immunofluorescence staining of full-thickness back skin sections from newborn pups at P0 of the indicated genotypes with antibodies against Krt6. Solid line indicates basement membrane. Scale bars, 10 µm. (**F**) Model: KRT1 promotes epidermal barrier formation and regulates the innate immune system by controlling inflammasome activation.

Table S1. Global comparison analyses of genome-wide transcriptional profiling data sets from ***Krt1* E18.5 skin***versus* atopic eczema (AE), psoriasis, *Krt5* P0 skin and epidermolysis bullosa simplex (EBS) skin. Shown are the differentially expressed genes (up- and down-regulated) that are similarly regulated (cut-off 2-fold).

No.	***Krt1* E18.5 *versus* AE**	***Krt1* E18.5 *versus* Psoriasis**	***Krt1* E18.5 *versus Krt5* P0**	***Krt1* E18.5 *versus* EBS**
1	ABCA12	ABCA12	2810417H13RIK	AREG
2	ACPP	ACPP	ADM	CHI3L1
3	ADM	ANKRD22	BTC	CXCL10
4	AQP7	ARG1	CXCR7	EGR2
5	AQP9	BLNK	EIF2S3Y	EPGN
6	ARC	CH25H	HSPA1B	HBEGF
7	ARG1	CHAC1	IFI202B	KLK6
8	AVPI1	CIDEC	IVL	KRT6B
9	BST2	CNFN	KRT16	SPRR2B
10	CDSN	COX7A1	KRT6A	SPRR2E
11	CH25H	CPA4	SERPINB2	SPRR4
12	COX7A1	CRABP2	SPRR1A	
13	CSTA	CXCL10	XIST	
14	CTH	DDX58	ZFP36	
15	DNASE1L3	DNASE1L3		
16	DSC1	DUSP14		
17	EGLN3	**ELOVL7**		
18	ELMOD1	**FABP5**		
19	FGFBP1	FGFBP1		
20	GJB2	GBP3		
21	GNA15	GDPD3		
22	GPD1	GJB2		
23	HOPX	GJB6		
24	**IL18**	GNA15		
25	IRF7	GPC6		
26	IRF9	GRHL3		
27	JUP	HPSE		
28	**KLK10**	HSD17B2		
29	**KLK5**	HYAL4		
30	**KLK6**	IFI27		
31	**KLK7**	IFI35		
32	KRT78	**IL1B**		
33	MLXIPL	**IL1F5**		
34	MX2	**IL1F6**		
35	OCLN	IPPK		
36	PLIN	IRF7		
37	PTGES	IRF9		
38	RAB38	IVL		
39	RHOD	KCTD11		
40	RPS13	**KLK10**		
41	**S100A9**	**KLK6**		
42	SCEL	**KLK7**		
43	SDCBP2	KRT16		
44	SERPINB2	KRT6A		
45	SLC15A3	KRT6B		
46	SLPI	KRT78		
47	SLURP1	LASS3		
48	**SPRR1A**	LYPD5		

49	**SPRR1B**	MX1		
50	**SPRR2G**	MX2		
51	**SPRR4**	OLFML1		
52	**TGM1**	OTUB2		
53	THUMPD1	PARP12		
54	TYRP1	PGLYRP4		
55	YOD1	PRSS22		
56		PRSS27		
57		RAB38		
58		RPTN		
59		RSAD2		
60		**S100A9**		
61		SDCBP2		
62		SLC18A2		
63		SLC26A9		
64		SLC27A4		
65		SLC39A6		
66		SLC7A11		
67		SLPI		
68		SLURP1		
69		SMOX		
70		SMPD3		
71		**SPRR1A**		
72		**SPRR1B**		
73		**SPRR2G**		
74		SQLE		
75		SRXN1		
76		SULT2B1		
77		TAP1		
78		TGM1		
79		TMEM40		
80		TMEM79		
81		TREX2		
82		USP18		
83		XKRX		
84		YOD1		
85		ZBTB16		
86		ZC3H12A		

Table S2. Global comparison analyses of genome-wide transcriptional profiling data sets from ***Krt1* P0 skin** *versus* atopic eczema (AE), psoriasis, *Krt5* P0 skin and epidermolysis bullosa simplex (EBS) skin. Shown are the differentially expressed genes (up- and down-regulated) that are similarly regulated (cut-off 2-fold).

No.	***Krt1* P0 *versus* AE**	***Krt1* P0 *versus* Psoriasis**	***Krt1* P0 *versus Krt5* P0**	***Krt1* P0 *versus* EBS**
1	ABCA12	ABCA12	ADM	AREG
2	ABCG1	ABCG1	BTC	ATP12A
3	ABI1	ACPP	CXCL1	COL14A1
4	ACPP	ADAM33	CXCL13	CXCL10
5	ADAM9	AFAP1L2	CXCL2	CXCL9
6	ADM	AMPD3	CXCR7	CYR61
7	ADRBK1	ANKRD22	CYR61	EPGN
8	AMPD3	AR	FOS	FOS
9	ANXA1	ARG1	H1FX	HBEGF
10	AQP9	ATP12A	HSPA1B	KLK6
11	ARC	ATP1A2	IER2	KRT6B
12	ARG1	ATP6V1C2	IFI202B	MFAP4
13	ASPN	BIRC3	IL6	PLA2G7
14	ATP1A2	C1QTNF2	IRF4	S100A8
15	ATP9A	CCL20	IVL	SPRR2A
16	AVPI1	CCNA2	KRT16	SPRR2B
17	B4GALT4	CD248	KRT6A	SPRR2E
18	BICD2	CEP55	SELE	SPRR4
19	BIN3	CFB	SERPINB2	
20	BIRC3	CH25H	SOCS3	
21	CAMK2N1	CHAC2	SPRR1A	
22	CAPN1	CLEC7A	SPRR3	
23	CAPNS1	CNFN	ZFP36	
24	CASP4	CPA4		
25	CCDC64	CRABP2		
26	CCNA2	CRYAB		
27	CDC123	CXCL1		
28	CDSN	CXCL10		
29	CFB	CXCL13		
30	CLINT1	CXCL9		
31	CLP1	CYP7B1		
32	CMYA5	DBN1		
33	CSTA	DDX58		
34	CTSS	DDX60		
35	CXCL1	DNASE1L3		
36	CXCL9	DUSP14		
37	CYP7B1	EFHD1		
38	CYR61	**ELOVL7**		
39	CYYR1	EPHX1		
40	DACT1	EPS8		
41	DDIT4L	**FABP5**		
42	DDX21	FCHSD1		
43	DEK	FGFBP1		
44	DHX16	G0S2		
45	DNASE1L3	GALNT6		
46	DPYD	GCH1		
47	DSC1	GJB2		
48	EAPP	GJB6		

49	EFEMP1	GRHL3		
50	EIF3A	GTF3C6		
51	EPN1	HIGD1A		
52	FABP5	HS3ST6		
53	FAM105A	HSD11B2		
54	FGFBP1	HSD17B2		
55	FGL2	HSPA4L		
56	FOS	HYAL4		
57	FPR2	IFI27		
58	FUT11	IGFBP6		
59	FZD1	IL13RA1		
60	GALNT6	IL17D		
61	GARNL1	IL19		
62	GCH1	**IL1B**		
63	GJB2	**IL1F5**		
64	GMFB	**IL1F6**		
65	HOPX	IL1RN		
66	HPGD	INA		
67	IDE	IPPK		
68	IER2	IRX1		
69	IL13RA2	ISLR		
70	IL1RN	IVL		
71	**IL6**	KCTD11		
72	IVL	**KLK6**		
73	IWS1	**KLK7**		
74	JUP	KPNA2		
75	KIFC3	KRT15		
76	**KLK5**	KRT16		
77	**KLK6**	KRT31		
78	**KLK7**	KRT6A		
79	KRT35	KRT6B		
80	KTN1	LASS3		
81	LAS1L	LCN2		
82	LRP1	LGR5		
83	MEGF9	LRG1		
84	MNDA	LRRC17		
85	MX2	LTF		
86	NAMPT	MFAP4		
87	NBR1	MFAP5		
88	NDFIP2	MFHAS1		
89	NOLA3	MX2		
90	OLFM4	MYADM		
91	OTUD6B	MYL9		
92	PDDC1	NAMPT		
93	PGAM1	NCAPG		
94	PHYHIP	NDRG4		
95	PLEKHG5	NFE2L3		
96	POSTN	NFKBIZ		
97	PPFIBP1	NME1		
98	PPP1R11	NOD2		
99	PSMC2	NPTX2		
100	PTGES	NRN1		
101	PTGES3	NUAK1		
102	RAB38	OAS2		
103	RAPGEF3	OBFC2A		
104	RG9MTD1	OLFML3		
105	RHOD	OTUB2		

106	RTP4	PALM		
107	**S100A9**	PARP12		
108	SAMHD1	PCNA		
109	SCYL2	PGLYRP4		
110	SDCBP2	PHYHIP		
111	SELL	PNPT1		
112	SERPINB2	POLR3G		
113	SF3A2	PPAP2B		
114	SFRP4	PPIF		
115	SH2D3C	PRDM1		
116	SIAH2	PRSS22		
117	SLC3A2	PRSS27		
118	SLPI	PYCARD		
119	SLURP1	RAB38		
120	**SOCS3**	RGMB		
121	SPON1	RHCG		
122	**SPRR1A**	RPL22L1		
123	**SPRR1B**	RPTN		
124	**SPRR2A**	RTP4		
125	**SPRR2G**	**S100A7A**		
126	**SPRR4**	**S100A8**		
127	SRGN	**S100A9**		
128	SUGT1	SDCBP2		
129	TACC3	SELE		
130	**TGM1**	SELL		
131	THBD	SHCBP1		
132	TMC4	SHISA2		
133	TMEM86A	SLC23A2		
134	TNFAIP3	SLC27A4		
135	TNP2	SLC29A1		
136	TPD52	SLC5A1		
137	TPM2	SLC7A11		
138	TRIM25	SLPI		
139	TSPAN3	SMPD3		
140	TSPAN7	**SPRR1A**		
141	TTC8	**SPRR1B**		
142	UBE2J1	**SPRR2G**		
143	UBE2K	**SPRR3**		
144	UBE2Z	SRXN1		
145	UCHL3	SULT2B1		
146	VPS26A	TACC3		
147	WFDC5	TGFA		
148	XIST	TGM1		
149	YDJC	THBD		
150	YOD1	TMEM79		
151	YTHDF3	TMEM86A		
152	ZBED4	TNNT1		
153	ZC3HAV1	TOP1		
154	ZXDB	TPPP3		
155		TREX2		
156		TRIP13		
157		TSPAN7		
158		TTK		
159		UBE2T		
160		UCHL3		
161		UCK2		
162		UGCG		

163 164 165 166		USP18 WFDC12 YOD1 ZC3H12A		

Table S3. Common identified differentially expressed genes present in AE, psoriasis and *Krt1* skin at E18.5 or P0 skin, or present in *Krt5* skin (P0), EBS and *Krt1* skin at E18.5 or P0 skin.

No.	Common genes identified in AE, Psoriasis and *Krt1* skin at E18.5	Common genes identified in AE, Psoriasis and *Krt1* skin at P0	Common genes identified in *Krt5* skin (P0), EBS and *Krt1* skin at E18.5	Common genes identified in *Krt5* skin (P0), EBS and *Krt1* skin at P0
1	ABCA12	ABCA12	-	CYR61
2	ACPP	ABCG1		
3	ARG1	ACPP		
4	CH25H	AMPD3		
5	DNASE1L3	ARG1		
6	FGFBP1	ATP1A2		
7	GJB2	CCNA2		
8	GNA15	CFB		
9	IRF7	CXCL1		
10	IRF9	CYP7B1		
11	KLK10	DNASE1L3		
12	KLK6	FABP5		
13	KLK7	FGFBP1		
14	KRT78	GALNT6		
15	MX2	GCH1		
16	RAB38	GJB2		
17	S100A9	IVL		
18	SDCBP2	KLK6		
19	SLPI	KLK7		
20	SLURP1	MX2		
21	SPRR1A	NAMPT		
22	SPRR1B	PHYHIP		
23	SPRR2G	RAB38		
24	TGM1	S100A9		
25	YOD1	SDCBP2		
26		SELL		
27		SLPI		
28		SPRR1A		
29		SPRR1B		
30		SPRR2G		
31		TACC3		
32		TGM1		
33		THBD		
34		TMEM86A		
35		TSPAN7		
36		UCHL3		
37		YOD1		

Table S4. Gene Sets from the Molecular Signaling Database (MSigDB), Gene Set Enrichment Analysis (GSEA), depicted in **Fig. 3F**.

Corresponding number in Fig. 2f	Gene Set from the Molecular Signaling Database (MSigDB), Gene Set Enrichment Analysis (GSEA), Broad Institute (http://www.broadinstitute.org/gsea/msigdb).
1	BIOCARTA_MONOCYTE_PATHWAY
2	BIOCARTA_LYM_PATHWAY
3	BIOCARTA_LAIR_PATHWAY
4	BIOCARTA_GRANULOCYTES_PATHWAY
5	KEGG_GRAFT_VERSUS_HOST_DISEASE
6	BIOCARTA_ERYTH_PATHWAY
7	BIOCARTA_STEM_PATHWAY
8	BIOCARTA_TH1TH2_PATHWAY
9	BIOCARTA_INFLAM_PATHWAY
10	REACTOME_CHEMOKINE_RECEPTORS_BIND_CHEMOKINES
11	BIOCARTA_CYTOKINE_PATHWAY
12	SA_MMP_CYTOKINE_CONNECTION
13	BIOCARTA_IL5_PATHWAY
14	ST_INTERFERON_GAMMA_PATHWAY
15	ST_INTERLEUKIN_13_PATHWAY
16	ST_IL_13_PATHWAY
17	ST_TYPE_I_INTERFERON_PATHWAY
18	BIOCARTA_SET_PATHWAY
19	SA_CASPASE_CASCADE
20	BIOCARTA_CASPASE_PATHWAY
21	BIOCARTA_MITOCHONDRIA_PATHWAY
22	BIOCARTA_UCALPAIN_PATHWAY
23	BIOCARTA_P35ALZHEIMERS_PATHWAY
24	BIOCARTA_MCALPAIN_PATHWAY
25	BIOCARTA_SPRY_PATHWAY
26	BIOCARTA_EGFR_SMRTE_PATHWAY
27	REACTOME_GRB2_EVENTS_IN_EGFR_SIGNALING
28	BIOCARTA_CARDIACEGF_PATHWAY
29	BIOCARTA_ARENRF2_PATHWAY
30	KEGG_NOD_LIKE_RECEPTOR_SIGNALING_PATHWAY
31	BIOCARTA_IL1R_PATHWAY
32	BIOCARTA_SODD_PATHWAY
33	REACTOME_JNK_PHOSPHORYLATION_AND_ACTIVATION_MEDIATED_BY_ ACTIVATED_HUMAN_TAK1
34	REACTOME_REGULATED_PROTEOLYSIS_OF_P75NTR
35	BIOCARTA_RANKL_PATHWAY
36	BIOCARTA_NFKB_PATHWAY
37	REACTOME_P75NTR_RECRUITS_SIGNALLING_COMPLEXES
38	REACTOME_HUMAN_TAK1_ACTIVATES_NFKB_BY_PHOSPHORYLATION_AND_ ACTIVATION_OF_IKKS_COMPLEX
39	REACTOME_P75NTR_SIGNALS_VIA_NFKB
40	REACTOME_NF_KB_IS_ACTIVATED_AND_SIGNALS_SURVIVAL
41	REACTOME_ACTIVATED_TAK1_MEDIATES_P38_MAP_ACTIVATION
42	BIOCARTA_CD40_PATHWAY
43	REACTOME_ACTIVATION_OF_THE_AP1_FAMILY_OF_TRANSCRIPTION_ FACTORS
44	REACTOME_VIRAL_DSRNA_TLR3_TRIF_COMPLEX_ACTIVATES_RIP1
45	REACTOME_TOLL_LIKE_RECEPTOR_4_CASCADE
46	REACTOME_TOLL_LIKE_RECEPTOR_9_CASCADE
47	REACTOME_ACTIVATED_TLR4_SIGNALLING

48	REACTOME_MYD88_CASCADE
49	BIOCARTA_GSK3_PATHWAY
50	BIOCARTA_PS1_PATHWAY
51	BIOCARTA_BCELLSURVIVAL_PATHWAY

Table S5. Used Pathway IDs for the ***Krt1*/AE pathway network analysis** (see also **Fig. 3F**). The first 100 MSigDB gene sets in hierarchical order were used to build up the pathway network.

No.	MSigDB Gene Sets (GSEA)	set_mean	p-value
1	REACTOME_XENOBIOTICS	0.342146156122824	0.00165990913
2	KEGG_LIMONENE_AND_PINENE_DEGRADATION	0.24192606961759	3,48E+09
3	REACTOME_CALCITONIN_LIKE_LIGAND_ RECEPTORS	0.240644032443641	4,11E+09
4	BIOCARTA_IL5_PATHWAY	0.226361191488986	0.00015500870
5	ST_INTERLEUKIN_13_PATHWAY	0.22274328827125	8,70E+09
6	ST_IL_13_PATHWAY	0.22274328827125	8,70E+09
7	BIOCARTA_FIBRINOLYSIS_PATHWAY	0.201704788830522	2,96E+07
8	REACTOME_ENDOGENOUS_STEROLS	0.184733140207795	3,50E+09
9	KEGG_GLYCOSAMINOGLYCAN_BIOSYNTHESIS_ KERATAN_SULFATE	0.178223464205867	2,11E+08
10	BIOCARTA_MONOCYTE_PATHWAY	0.172585065662414	8,71E+09
11	BIOCARTA_P35ALZHEIMERS_PATHWAY	0.172019966962239	1,83E+09
12	REACTOME_COMMON_PATHWAY	0.167850215932703	3,65E+09
13	BIOCARTA_SODD_PATHWAY	0.167135255215987	0.00010667654
14	SA_CASPASE_CASCADE	0.166192447500512	2,50E+09
15	BIOCARTA_GLYCOLYSIS_PATHWAY	0.159556884840773	0.00010751727
16	KEGG_FOLATE_BIOSYNTHESIS	0.1577448096543	5,94E+08
17	BIOCARTA_RANMS_PATHWAY	0.157544325953145	3,56E+09
18	BIOCARTA_LYM_PATHWAY	0.150095870010906	0.00012524692
19	REACTOME_FACILITATIVE_NA_INDEPENDENT_ GLUCOSE_TRANSPORTERS	0.136469526257328	3,99E+09
20	BIOCARTA_RANKL_PATHWAY	0.136260711590791	1,88E+09
21	REACTOME_P75NTR_RECRUITS_SIGNALLING_ COMPLEXES	0.133476097568378	4,91E+09
22	KEGG_NITROGEN_METABOLISM	0.132316579166059	4,03E+08
23	SA_MMP_CYTOKINE_CONNECTION	0.129880590714409	9,14E+09
24	BIOCARTA_CYTOKINE_PATHWAY	0.127982359463972	4,16E+09
25	REACTOME_GAP_JUNCTION_ASSEMBLY	0.126080386692963	3,68E+08
26	BIOCARTA_STEM_PATHWAY	0.123568305183963	0.00011125699
27	KEGG_BIOSYNTHESIS_OF_UNSATURATED_ FATTY_ACIDS	0.122305282427811	5,33E+09
28	KEGG_GLYCOSPHINGOLIPID_BIOSYNTHESIS_ LACTO_AND_NEOLACTO_SERIES	0.121955041092212	2,42E+09
29	KEGG_VALINE_LEUCINE_AND_ISOLEUCINE_ BIOSYNTHESIS	0.119750162405712	5,51E+09
30	BIOCARTA_GRANULOCYTES_PATHWAY	0.119165481041174	7,02E+09
31	REACTOME_PYRIMIDINE_CATABOLISM	0.11676117519777	0.00013688546
32	BIOCARTA_CASPASE_PATHWAY	0.115231569002805	3,48E+09
33	REACTOME_OPSINS	0.110744389638012	0.00262739405
34	REACTOME_NF_KB_IS_ACTIVATED_AND_ SIGNALS_SURVIVAL	0.109909838777692	6,91E+09
35	REACTOME_RECRUITMENT_OF_NUMA_TO_ MITOTIC_CENTROSOMES	0.109685100496436	0.00023496594
36	REACTOME_MYD88_CASCADE	0.109635628106054	1,49E+09
37	REACTOME_P75NTR_SIGNALS_VIA_NFKB	0.109193784876127	2,33E+09
38	REACTOME_STEROID_HORMONE_BIOSYNTHESIS	0.108439693936905	9,80E+09
39	KEGG_RIBOFLAVIN_METABOLISM	0.106479209022272	5,40E+09
40	BIOCARTA_SET_PATHWAY	0.10391096233981	0.00017940001
41	BIOCARTA_BCELLSURVIVAL_PATHWAY	0.103690346226528	7,96E+09

42	KEGG_NOD_LIKE_RECEPTOR_SIGNALING_PATHWAY	0.101286626335841	3,25E+09
43	BIOCARTA_CD40_PATHWAY	0.101200117150136	3,08E+09
44	REACTOME_BASIGIN_INTERACTIONS	0.100287993889088	2,88E+09
45	REACTOME_CHEMOKINE_RECEPTORS_BIND_CHEMOKINES	0.099014578777434	2,39E+09
46	REACTOME_HDL_MEDIATED_LIPID_TRANSPORT	0.099004381118123	0.00044979053
47	KEGG_GRAFT_VERSUS_HOST_DISEASE	0.09629338657181	4,66E+09
48	ST_INTERFERON_GAMMA_PATHWAY	0.095078481418381	0.00013873475
49	ST_TYPE_I_INTERFERON_PATHWAY	0.094417954374085	0.00049409140
50	BIOCARTA_MCALPAIN_PATHWAY	0.093598211909839	2,21E+09
51	REACTOME_REGULATION_OF_RHEB_GTPASE_ACTIVITY_BY_AMPK	0.093532082760991	0.00015591529
52	BIOCARTA_ERYTH_PATHWAY	0.092768551454143	6,51E+09
53	REACTOME_GLUTATHIONE_CONJUGATION	0.092750650610776	2,58E+09
54	BIOCARTA_EIF_PATHWAY	0.091911841603297	0.00014632355
55	BIOCARTA_NEUROTRANSMITTERS_PATHWAY	0.090605848773247	0.00364247330
56	BIOCARTA_LAIR_PATHWAY	0.090113651327229	7,06E+09
57	REACTOME_ACTIVATION_OF_THE_AP1_FAMILY_OF_TRANSCRIPTION_FACTORS	0.089418954052513	0.00010769480
58	REACTOME_PROSTANOID_HORMONES	0.087911017966067	0.00023122360
59	BIOCARTA_MITOCHONDRIA_PATHWAY	0.087836944414960	9,34E+09
60	REACTOME_CHYLOMICRON_MEDIATED_LIPID_TRANSPORT	0.085841841781653	2,50E+09
61	REACTOME_FORMATION_OF_TUBULIN_FOLDING_INTERMEDIATES_BY_CCT_TRIC	0.085683896382995	3,62E+09
62	REACTOME_HUMAN_TAK1_ACTIVATES_NFKB_BY_PHOSPHORYLATION_AND_ACTIVATION_OF_IKKS_COMPLEX	0.085637787211490	4,77E+09
63	KEGG_PANTOTHENATE_AND_COA_BIOSYNTHESIS	0.084851426525908	0.00010062772
64	REACTOME_CDC6_ASSOCIATION_WITH_THE_ORC:ORIGIN_COMPLEX	0.083494760373342	8,77E+08
65	BIOCARTA_ARENRF2_PATHWAY	0.082720451375794	7,41E+09
66	REACTOME_JNK_PHOSPHORYLATION_AND_ACTIVATION_MEDIATED_BY_ACTIVATED_HUMAN_TAK1	0.082484459082167	0.00016915744
67	REACTOME_BILE_SALT_AND_ORGANIC_ANION_SLC_TRANSPORTERS	0.082467888824695	0.00021190194
68	REACTOME_VIRAL_DSRNA_TLR3_TRIF_COMPLEX_ACTIVATES_RIP1	0.082234932521885	4,07E+09
69	REACTOME_TOLL_LIKE_RECEPTOR_9_CASCADE	0.081018300016788	1,39E+09
70	BIOCARTA_NUCLEARRS_PATHWAY	0.080774163106227	6,59E+08
71	BIOCARTA_SPRY_PATHWAY	0.080330479048979	3,02E+09
72	BIOCARTA_INFLAM_PATHWAY	0.080079201672178	2,72E+09
73	SA_REG_CASCADE_OF_CYCLIN_EXPR	0.078933049720256	0.00014391206
74	BIOCARTA_CARDIACEGF_PATHWAY	0.078332441106146	4,15E+09
75	BIOCARTA_TH1TH2_PATHWAY	0.078044001743851	7,02E+08
76	BIOCARTA_EGFR_SMRTE_PATHWAY	0.077842365640785	0.00020147834
77	REACTOME_POST_CHAPERONIN_TUBULIN_FOLDING_PATHWAY	0.077593536646745	7,41E+09
78	BIOCARTA_VITCB_PATHWAY	0.077492291543725	0.00014272211
79	REACTOME_ACTIVATED_TLR4_SIGNALLING	0.076547789461690	1,46E+09
80	REACTOME_FORMATION_OF_FIBRIN_CLOT_CLOTTING_CASCADE	0.076162267563133	2,55E+09
81	REACTOME_CYTOCHROME_P450_ARRANGED_BY_SUBSTRATE_TYPE	0.075567109603781	2,77E+09

82	REACTOME_SIGNALING_BY_TGF_BETA	0.075460853450406	6,86E+09
83	REACTOME_NOTCH_HLH_TRANSCRIPTION_PATHWAY	0.074571042954623	9,01E+09
84	REACTOME_ASSOCIATION_OF_LICENSING_FACTORS_WITH_THE_PREREPLICATIVE_COMPLEX	0.073839561099066	9,21E+09
85	KEGG_PROXIMAL_TUBULE_BICARBONATE_RECLAMATION	0.073524681376697	3,74E+09
86	REACTOME_ACTIVATED_TAK1_MEDIATES_P38_MAPK_ACTIVATION	0.073510516175143	0.00019939489
87	REACTOME_PREFOLDIN_MEDIATED_TRANSFER_OF_SUBSTRATE_TO_CCT_TRIC	0.073442878343503	2,26E+09
88	REACTOME_NEF_MEDIATED_DOWNREGULATION_OF_MHC_CLASS_I_COMPLEX_CELL_SURFACE_EXPRESSION	0.072482685086789	0.00030626796
89	BIOCARTA_NFKB_PATHWAY	0.071138451224358	4,29E+09
90	BIOCARTA_UCALPAIN_PATHWAY	0.070887728057342	0.00017826673
91	KEGG_CIRCADIAN_RHYTHM_MAMMAL	0.070778965013227	0.00013064063
92	BIOCARTA_GSK3_PATHWAY	0.070705985676147	6,79E+08
93	REACTOME_TOLL_LIKE_RECEPTOR_4_CASCADE	0.070138746193596	8,82E+08
94	REACTOME_GRB2_EVENTS_IN_EGFR_SIGNALING	0.07008576283745	0.00011014069
95	BIOCARTA_IL1R_PATHWAY	0.069333075590814	1,08E+09
96	REACTOME_REGULATED_PROTEOLYSIS_OF_P75NTR	0.068519125990304	0.00010526413
97	BIOCARTA_PS1_PATHWAY	0.068362602987295	0.00017409888
98	REACTOME_LIPOPROTEIN_METABOLISM	0.067985368915951	7,09E+09
99	BIOCARTA_AHSP_PATHWAY	0.067516022033075	0.00025177868
100	KEGG_NICOTINATE_AND_NICOTINAMIDE_METABOLISM	0.067392451165054	2,59E+09

Table S6.*Krt1* PCR genotyping strategy.

ID	Primer (5'□3')
BN5	AGCCTACCCTCTGGTAGATTGTCG
BN280	ACTATCCTACATCCTAGGAC ATCTTAGGGAGG
BN281	CAGTTCAAGAGCTCAGTGATAATGCAGTG GGATG

PCR was performed with Phusion DNA polymerase (Finnzymes).
94°C for 5 min; 35 cycles of 94°C for 15 sec, 65°C for 30 sec, 72°C for 3 min; final extension 72°C for 7 min.
DNA fragment size for the wildtype allele: 3.5 kb.
DNA fragment size for the mutant allele: 2.8 kb.

Table S7. Antibodies.

Primary antibody	Host	Source
Anti-KRT1, clone 34betaB4	Mouse	Enzo Life Sciences
Anti-Krt1, AF109	Rabbit	Covance
Anti-KRT10, clone DE-K10	Mouse	Dako
Anti-KRT5 head domain	Guinea pig	Betz et al., 2006[a]
Anti-Krt5	Rabbit	Generated against a C-terminal peptide
Anti-KRT14	Rabbit	Generated against a C-terminal peptide
Anti-KRT6, monoclonal	Mouse	Progen, Heidelberg
Anti-Krt16	Rabbit	P.A. Coulombe, Baltimore, MD
Anti-loricrin, AF62	Rabbit	Covance
Anti-involucrin	Rabbit	Covance
Anti-filaggrin, AF111	Rabbit	HiSS Diagnostics
Anti-Mrp8 and anti-Mrp14	Rabbit	J. Roth, Münster, Germany
Anti-PECAM (CD31), monoclonal	Mouse	N. Koch, Cologne, Germany
Anti-IL-18, clone 93-10C	Rat	R&D Systems
Anti-caspase-1, A-19	Rabbit	Santa Cruz Biotechnology
Anti-β-Actin	Mouse	Sigma
Secondary antibody		
Anti-mouse-Cy2, -Cy3 IgG	Donkey	Invitrogen and Dianova, Hamburg
Anti-rabbit-Cy2, -Cy3 IgG	Donkey	Invitrogen and Dianova, Hamburg
Anti-rat-Cy2, -Cy3 IgG	Donkey	Invitrogen and Dianova, Hamburg
Anti-guinea-pig-Cy2, -Cy3 IgG	Donkey	Invitrogen and Dianova, Hamburg

[a]Betz, R.C. *et al.* Loss-of-function mutations in the keratin 5 gene lead to Dowling-Degos disease. *Am. J. Hum. Genet.* 78, 510-519 (2006).

Table S8. Mouse qPCR primer sequences.

Gene	Forward primer (5'□3')	Reverse primer (5'□3')	Size (bp)
Tslp[a]	CGACAGCATGGTTCTTCTCA	CGATTTGCTCGAACTTAGCC	170
Defb3 [b]	GCTTCAGTCATGAGGATCCATT	CTGCCTCCTTTCCTCAAACA	119
S100A8 [b]	TCACCATGCCCTCTACAAGA	GCATTGTCACTATTGATGTCCAA	120
S100A9 [b]	TCAGACAAATGGTGGAAGCA	GCTCAGCTGATTGTCCTGGT	116
Slpi [b]	GCCTTCACCATGAAGTCCT	AGGGCAGGCTCCGATTTT	120
Il18	TGGCCCAGGAACAATGGCTGC	TGCGGTTGTACAGTGAAGTCGGC	148
Il33	TCCCCGGCAAAGTTCAGCAGC	TGGTGAGGCCAGAACGGAGTCT	127
K16	GCAGCTGGCTCAGCTTCGCT	GGAGTGCTGTGAGGAGGAGTGGA	148
Lce3c	TCTTCTCCTGCCTTTGCTGT	GAGCACTTTGGAGAGGGACA	107
Lce3f	GCCTTCTTCTCCTACCTTTGC	GCAGACACTGTGTTGTGCTCT	149
Rptn	GCTGCTGCTCACTGAGTTTG	GACCAATTGGAATACCAGCA	149
18S RNA[c]	GTAACCCGTTGAACCCCATT	CCATCCAATCGGTAGTAGCG	150

[a]Briot, A. *et al.* Kallikrein 5 induces atopic dermatitis-like lesions through PAR2-mediated thymic stromal lymphopoietin expression in Netherton syndrome. *J. Exp. Med.*206, 1135-1147 (2009).
[b]de Guzman Strong, C. *et al.* Lipid defect underlies selective skin barrier impairment of an epidermal-specific deletion of Gata-3. *J. Cell Biol.* 175, 661-670 (2006).
[c]Aberg, K.M. *et al.* Co-regulation and interdependence of the mammalian epidermal permeability and antimicrobial barriers. *J. Invest. Dermatol.* 128, 917-925 (2008).

Table S9. SiRNAs used for knock-down experiments (Sigma-Aldrich).

ID	**Sequence (5'□3')**
Scramble	UUCUCCGAACGUGUCACGUTT
Casp-1	GGCAGAGAUUUAUCCAAUATT
K1-1 (*Krt1*)	CAGGAAAUUGAUUUCCUUAdTdT
K1-2 (*Krt1*)	GACUUAGAUCUGAAAUCG AdTdT
K1-3 (*Krt1*)	GUCGAUUUGUCCCAGCCU UdTdT
K1-4 (*Krt1*)	CCCAUAAUUUAGAGCCCUAdTdT3

Table S10. Sample size, statistical tests and p-values of experimental data.

Figure	Analysis	n	Normality test	Statistical test	Alpha	*P*
Fig. 2D	TEWL	wt n=38 het n=83 ko n=43	failed ($P<0.05$) (Shapiro-Wilk)	ANOVA on ranks (Kruskal-Wallis) Pairwise multiple comparison (Dunn's method)		$P<0.001$ wt vs ko: $P<0.05$ het vs ko: $P<0.05$
Fig. 2E	CE counts	n=3	passed ($P=0.158$)	Unpaired t-test	alpha=0.05 power: 1,000	$P<0.001$
Fig. 4D	IL-18 serum	pooled n=28	passed ($P=0.801$)	Unpaired t-test	alpha=0.05 power: 0.864	$P=0.024$
	IL-18 epid. extr.	pooled n=6	passed ($P=0.314$)	Unpaired t-test	alpha=0.05 power: 0.058	$P=0.477$
	IL-33 serum	pooled n=28	passed ($P=0.972$)	Unpaired t-test	alpha=0.05 power: 0.997	$P=0.008$
	IL-33 epid. extr.	pooled n=6	passed ($P=0.909$)	Unpaired t-test	alpha=0.05 power: 0.997	$P=0.008$
	S100A8/ S100A9 serum	pooled n=28		Unpaired t-test	alpha=0.05 power: 0.204	$P=0.149$
	S100A8/ S100A9 epid. extr.	pooled n=6		Unpaired t-test	alpha=0.05 power: 1.0	$P<0.001$
Fig. 4E	IL-18 ELISA	pools see Fig. legend		One way ANOVA (Holm-Sidak method)	alpha=0.05 power: 1.0	wt P0 vs ko P0: $P<0.001$ het P0 vs ko P0: $P<0.001$ wt IgG1 vs het Ab: $P<0.001$ wt IgG1 vs ko Ab: $P<0.001$
Fig. 4G	CE counts	see Fig. legend	passed ($P=0.763$)	One way ANOVA (Holm-Sidak method)	alpha=0.05 power: 1.0	wt IgG1 vs ko control: $P<0.001$ wt IgG1 vs ko Ab: $P<0.001$ wt Ab vs ko control: $P<0.001$ wt Ab vs ko Ab: $P<0.001$ ko Ab vs ko control: $P=0.014$ wt IgG1 vs wt Ab: $P=0.069$
Fig. 5E	CE counts	n=3	Passed ($P=0.177$)	One way ANOVA (Holm-Sidak method)	alpha=0.05 power: 1.0	$Krt1^{+/+}$ vs $Krt1^{-/-}$: $P<0.001$ $Krt1^{+/+}$ vs $Krt1^{-/-}$ $S100A9^{-/-}$: $P<0.001$ $Krt1^{+/+}S100A9^{-/-}$ vs $Krt1^{-/-}S100A9^{-/-}$: $P<0.001$

Fig. 5E cont.						$Krt1^{+/+}S100A^{-/-}$ vs $Krt1^{-/-}$: $P<0.001$ $Krt1^{+/+}Il18^{-/-}$ vs $Krt1^{-/-}S100A9^{-/-}$: $P<0.001$ $Krt1^{+/+}Il18^{-/-}$ vs $Krt1^{-/-}$: $P<0.001$ $Krt1^{+/+}$ vs $Krt1^{-/-}$ $Il18^{-/-}$: $P<0.001$ $Krt1^{+/+}S100A9^{-/-}$ vs $Krt1^{-/-}Il18^{-/-}$: $P<0.001$ $Krt1^{+/+}Il18^{-/-}$ vs $Krt1^{-/-}Il18^{-/-}$: $P<0.001$ $Krt1^{-/-}Il18^{-/-}$ vs $Krt1^{-/-}S100A9^{-/-}$: $P<0.001$ $Krt1^{-/-}Il18^{-/-}$ vs $Krt1^{-/-}$: $P=0.013$
Fig. S3C	Lce3c E18.5	n=3	passed ($P=0.235$)	Unpaired t-test	alpha=0.05 power: 0.792	$P=0.019$
	Lce3f E18.5	n=3	passed ($P=0.311$)	Unpaired t-test	alpha=0.05 power: 0.543	$P=0.044$
	Rptn E18.5	n=3	passed ($P=0.124$)	Mann-Whitney Rank Sum test		$P=0.100$
	Lce3c nb	n=3	passed ($P=0.199$)	Unpaired t-test	alpha=0.05 power: 0.404	$P=0.069$
	Lce3f nb	n=3	passed ($P=0.199$)	Unpaired t-test	alpha=0.05 power: 0.325	$P=0.091$
	Rptn nb	n=3	passed ($P=0.146$)	Unpaired t-test	alpha=0.05 power: 0.989	$P=0.004$
Fig. S3D	Il18 E18.5	n=3	passed ($P=0.665$)	Unpaired t-test	alpha=0.05 power: 0.941	$P=0.008$
	Il33 E18.5	n=3	passed ($P=0.157$)	Unpaired t-test	alpha=0.05 power: 0.999	$P=0.002$
	Il18 nb	n=3	passed ($P=0.171$)	Unpaired t-test	alpha=0.05 power: 0.052	$P=0.370$
	Il33 nb	n=3	passed ($P=0.087$)	Unpaired t-test	alpha=0.05 power: 0.092	$P=0.274$
Fig. S3E	Tslp E18.5	n=3	passed ($P=0.133$)	Mann-Whitney Rank Sum test		$P=0.100$
	S100A8 E18.5	n=3	passed ($P=0.938$)	Mann-Whitney Rank Sum test		$P=0.700$
	S100A9 E18.5	n=3	passed ($P=0.809$)	Mann-Whitney Rank Sum test		$P=0.400$
	Tslp nb	n=3	passed ($P=0.092$)	Unpaired t-test	alpha=0.05 power: 0.458	$P=0.058$
	S100A8 nb	n=3	passed ($P=0.282$)	Unpaired t-test	alpha=0.05 power: 0.296	$P=0.102$
	S100A9 nb	n=3	passed ($P=0.281$)	Unpaired t-test	alpha=0.05 power: 0.275	$P=0.110$
Fig. S4B	PECAM + quant.	n=3	passed ($P=0.554$)	Unpaired t-test	alpha=0.05 power: 1.0	$P<0.001$